The Effect of Seamount Subduction on the Formation of Holocene Marine Terraces: A Comparison of Kinematic and Mechanical Plate Subduction Models

J. Komori[1], R. Ando[2], S. Miura[3], and R. Arai[3]

[1]Earth Observatory of Singapore, Nanyang Technological University, 50 Nanyang Avenue, Singapore.

[2]Department of Earth and Planetary Science, School of Science, University of Tokyo, 7-3-1 Hongo, Bunkyo-ku, Tokyo, Japan

[3]Research Institute for Marine Geodynamics, Japan Agency for Marine-Earth Science and Technology, 3173-25, Showa-machi, Kanazawa-ku, Yokohama, Kanagawa, Japan

Corresponding author: Junki Komori (junki.komori@ntu.edu.sg)

Key Points:

- Traditional plate subduction models fall short in explaining Holocene marine terrace formation.
- A novel mechanical model addresses stress changes and deformations near a subducted seamount.
- Assessing megathrust earthquakes using Holocene marine terraces must account for plate interface irregularities.

Abstract

Marine terraces have long been a subject of paleoseismology to reveal the rupture history of megathrust earthquakes. However, the mechanisms underlying their formation, in relation to crustal deformation, have not been adequately explained by kinematic models. A key challenge has been that the uplifted shoreline resulting from a megathrust earthquake tends to subside back to sea level during subsequent interseismic periods. This study focuses on the remaining permanent vertical deformation resulting from steady plate subduction and examines it quantitatively using three plate subduction models. Specifically, we pay attention to the effects of irregular geometries in the plate interface, such as subducted seamounts. Besides a simplified model examination, this study employs the plate geometry around the Sagami trough, central Japan, to compare with surface deformation observation. The subduction models employed are the kinematic subducting plate model, the elastic/viscoelastic fault model, and the mechanical subducting plate model (MSPM). The MSPM, introduced in this study, allows for more realistic simulations of crustal displacements by imposing net zero shear stress change on the plate boundary. Notably, the presence of a subducted seamount exerts a significant influence on surface deformation, resulting in a concentrated permanent uplift above it. The simulation of earthquake sequence demonstrates that coseismic uplifts can persist over time and contribute to the formation of marine terraces. The results demonstrated that the geological observations of coseismic and long-term deformations can be explained by the influence of a subducted seamount, previously identified in seismic surveys.

Plain Language Summary

This study explores how marine terraces are created resulting from plate subduction. Existing models struggle to explain why these terraces persist. In traditional models, the ground lifted during earthquakes sink back by the same amount after the earthquake, but this doesn't match real observations. In this study, we used a simulation to understand the crustal deformation around the plate subduction zone. Specifically, we looked at how uplift happens when there is an irregularity on the plate boundary. Because previous models did not consider the effects of such irregularity, we also made a new subduction model. As a result, we found irregularities on plate boundary can lead to permanent deformation that is more significant than in the previous simulation. testing our model on the Boso Peninsula in central Japan, the simulated deformation matched real observation of marine terraces. This research highlights the importance of considering plate geometry when studying the crustal deformation and earthquake history using marine terraces.

1 Introduction

Accurate assessment of the seismic hazard of a particular area requires a thorough understanding of the past earthquakes that have occurred on the relevant fault. However, the intervals between great earthquakes can span hundreds or even thousands of years, exceeding the range of modern instrumental observations which are typically limited to around one hundred years at best. Consequently, we must rely on historical records and geological data to reveal earthquake occurrence histories.

Holocene marine terraces are widely recognized as an important geological record of past large earthquakes, especially around subduction zones. When megathrust earthquakes occur along subduction zones, they can generate intense uplifts and subsidence in the surrounding areas. Such uplifts may create a stair-case coastal landform by emerging a beach and wave-cut bench. This phenomenon has been observed in recent earthquakes such as the 1923 Taisho Kanto earthquake (Shishikura, 2014), the 2004 and 2005 Sunda megathrust earthquakes (Briggs et al., 2006), and

the 2016 Kaikoura earthquake (Clark et al., 2017). While some of these uplift events include movements on upper plate faults branching from the plate interface (e.g., Clark et al., 2017), others are attributed to slips on the plate interfaces. Recurrence of such uplifts over time can lead to the development of Holocene marine terraces, which have been observed on various coasts around subduction zones and studied extensively seeking to understand earthquake recurrence (Shimazaki and Nakata, 1980; Ramos and Tsutsumi, 2010; Wang et al., 2013; Litchfield et al., 2020), including those attributed to upper plate faulting. Therefore, the Holocene marine terraces are highly valuable records for investigating past megathrust earthquakes.

However, the approach of using marine terraces to investigate past earthquake recurrence has been subject to questions. While the uplift accumulation can be explained by slip recurrence on a fault when coseismic deformations are attributed to intraplate faulting (e.g., Ninis et al., 2023), understanding the formation of marine terraces uplifted due to interplate slip is not straightforward. Specifically, the back-slip model, which is a well-known kinematic model for crustal deformation resulting from earthquake recurrences along subduction zones developed by Savage (1983), assumes that the coseismic slip and interseismic back-slip are equal in magnitude but opposite in direction, resulting in a net zero amount of slip on the fault after an earthquake sequence. This assumption suggests that the total amount of crustal deformation will also be net zero, when elastic deformation is assumed. As a result, the formation of marine terraces is deemed unlikely under this model.

The existence of marine terraces along various coasts without significant upper plate faulting raises questions about the permanent uplift resulting from plate subduction. One explanation for this uplift was proposed by Sato and Matsu'ura (1988), who suggested that steady subduction can generate permanent vertical deformation through fault slip in an elastic-viscoelastic stratum. Fukahata and Matsu'ura (2006; 2016) indicated that this permanent deformation is caused by the interaction between the curvature of plate interface and gravitational compensation. In addition, Kanda and Simons (2010; 2012) proposed that an elastic model can account for permanent vertical deformation by assuming steady slips on the upper and lower interfaces of the subducting slab, resulting from the effect of plate bending. While these models focused on long-term deformations and did not distinguish into individual earthquake sequences, the accumulation of deformations resulting from earthquake sequences should ultimately yield the same distribution.

However, these models focus on longer spatial and temporal scales of over 100 km and 10–100 thousand years, which are more relevant to great-scale terrains such as island arcs. To study the deformation later than the Holocene glacial retreat (<10k years BP) and its impact on marine terraces, the paleo-seismological investigations must focus on smaller-scale spatiotemporal deformation histories. Recent geological investigations of marine terraces have yielded essential observations. For example, the Holocene marine terraces on the southernmost tip of the Boso Peninsula in central Japan (Figure 1) indicated that their elevation distribution abruptly decreases within a short distance and its typical wavelength ranges 5–10 km (Komori et al., 2021). Furthermore, these marine terraces showed elevation changes along the strike direction of the subduction zone, indicating inhomogeneity in the subduction geometry.

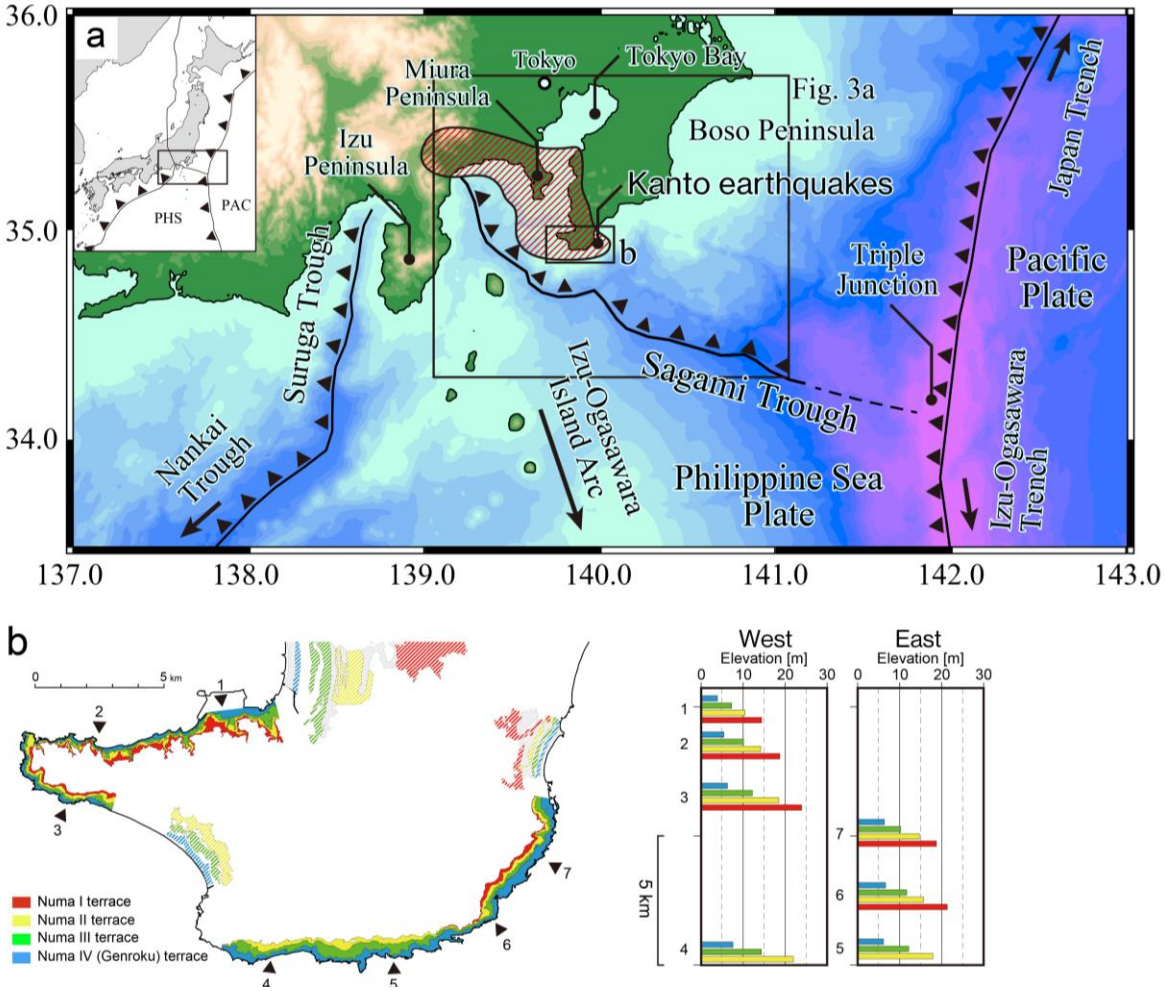

Figure 1. Survey region of this study and geological observations. (a) Tectonic setting of the Sagami Trough. The red meshed area indicates the estimated source region of the historical Kanto earthquakes (Sato et al., 2005; Sato et al., 2016). (b) Distribution of the Numa terraces after Komori et al. (2020). Right panels show the elevation distribution of the Numa terraces at each reference point, indicated by triangles in the left map.

Many previous studies have focused on the influence of plate interface irregularities on various tectonic and seismological phenomena (e.g., Wang and Bilek, 2011). Specifically, the subduction of seamounts has been explored through various model simulations, including its impact on the tectonic formation of accretionary prisms (Miyakawa et al., 2020) and its effects on earthquakes, including slow slip events, resulting from the irregular geometry and fluid intrusion (van Rijsingen et al., 2018; Sun et al., 2020). However, the investigation of crustal deformation due to subduction over timeframes ranging from 1,000 to 10,000 years, which is the focus of this study, has not received sufficient attention through quantitative model simulations. This timescale falls in a middle ground between the previous objectives, where the deformation is transient and negligible compared to that in active tectonic structures, while the sequence of coupling and rupture can be approximately averaged. Consequently, modeling of plate subduction involving multiple

earthquake sequences and mechanically consistent crustal deformation model over a millennium scale is required.

Regarding crustal deformation, the impact of subducting seamounts on the surface and seafloor geometry has been suggested by analogue experiments (Dominguez et al., 1998; 2000) and geological observations (Kodaira et al., 2000; Gardner et al., 2001). The long-term deformation can be broken down into an accumulation of deformations resulting from individual earthquake sequences. Therefore, such long-term deformation patterns are presumed to reflect the asymmetry of deformation between inter- and coseismic periods. Given the significance of understanding the deformation sources for interpreting Holocene marine terraces, it is imperative to conduct a quantitative investigation of the effects of subducted seamounts over timescales spanning thousands of years.

In the Sagami Trough subduction zone, the target region of this study, a seismic reflection survey detected the bump geometry of a subducted seamount (Tsumura et al., 2009), and its effect on crustal deformation has been discussed (Sato et al., 2016). However, previous modeling investigations have encountered the difficulty in simulating the formation of the Holocene marine terraces, which was possibly resulted from the assumption of smooth plate interface geometry and underestimation of the effect due to interface irregularities.

We conducted a modeling study on crustal deformation concerning marine terrace formation, which is resulting from plate subduction. Recognizing the inadequacy of previous models to explain residual uplift following earthquake sequences, we started with a simple modeling examination to establish the asymmetry of crustal deformation distribution between interseismic coupling and coseismic rupture, rather than relying on individual case studies. The suspected factor contributing to this asymmetry is irregular geometry at the plate interface. However, since traditional subduction models often implicitly assume a smooth interface geometry, introducing irregularities into such models may lead to mechanically inconsistent assumptions and potential misinterpretation of crustal deformation.

To address this concern, this study proposed a mechanically consistent subduction model designed to accommodate complex plate interface geometries, including irregularities such as subducted seamounts, and evaluated its impact on simulated deformation with a simple modeled subduction geometry. Finally, we compared the long-term vertical deformation distribution observed in the Boso Peninsula with the model simulation results, discussing the significance of plate interface geometry in assessing crustal deformation histories around subduction zones.

2 Sagami Trough Subduction Zone

The Sagami Trough is a convergent plate boundary where the Philippine Sea Plate (PHS) subducts in a northwestward direction beneath the continental plate of northeast Japan at a rate of approximately 30–40 mm per year (Seno et al., 1993; DeMets et al., 1994) (Figure 1a). This subduction zone exhibits a highly complex geometry, with the eastern and western ends marked by the triple junction, where the Pacific Plate subducts below the PHS, and the Izu Peninsula, a collided volcanic island, respectively. Historical documents record the occurrence of two interplate earthquakes along this plate boundary: the 1703 M8.2 Genroku Kanto earthquake and the 1923 M7.9 Taisho Kanto earthquake (hereafter, the 1703 Genroku earthquake and the 1923 Taisho earthquake, respectively) (Usami et al., 2013). The 1923 Taisho earthquake caused an uplift of approximately 2 m in the coastal area around Sagami Bay. Additionally, geological evidence shows that the southernmost tip of the Boso Peninsula experienced an uplift of approximately 6 m during the 1703 Genroku earthquake. While we have built less consensus about the interval times

of the Kanto earthquakes, the elastic recovery of these earthquakes probably has not been fully completed. The source fault of the 1923 Taisho earthquake is broadly acknowledged to be on the upper boundary of PHS from geodetic and teleseismic inversions (Sato et al., 2005; Nyst et al., 2006). While some geodetic inversion argued a possibility of activation of an inland fault (Pollitz et al., 1996), subsequent geological studies have proved no recent activity on the corresponding faults.

In addition to the marine terraces formed in historical era, older uplifted coasts are also recognized at the southernmost part of the Boso peninsula. These terraces, known as the Numa terraces, have been the subject of numerous geological and geomorphological studies. (Watanabe, 1929; Matsuda et al., 1978; Nakata et al., 1980; Kawakami and Shishikura, 2006; Komori et al., 2020; 2021) (Figure 1b). The Numa terraces are classified into four levels, namely Numa I, II, III, and IV in descending order (Nakata et al., 1980). The lowest one, Numa IV, is the uplifted coast caused by the 1703 Genroku earthquake. The distribution pattern of these terrace platforms suggests that the Numa terraces likely represent records of similar type >M8 class megathrust earthquakes, referred to as Genroku-type earthquakes. Besides the Genroku-type earthquakes, there are also earthquakes that occur more frequently but cause minor uplift up to 1–2 m. Beach ridges distributed along the western coast of the Boso peninsula imply the recurrence of earthquakes similar to the 1923 Taisho earthquake (Shishikura, 2014).

Previous studies have extensively discussed the formation scenario of the Numa terraces and the occurrence history of the Kanto earthquakes. Some of these earlier studies, such as Matsuda et al. (1978), attempted to correlate the distribution of Numa terraces with the pattern of coseismic uplift and interseismic subsidence associated with historical earthquakes. However, the similarity in the spatial distribution of marine terraces does not necessarily provide straightforward evidence for the recurrence of characteristic earthquakes because the influence of interseismic deformation is much greater than the variation in coseismic deformations. Sato et al. (2016) explored the permanent uplifts caused by the plate subduction at the southernmost Boso peninsula. They used the kinematic formula within an elastic/viscoelastic half-space (Sato and Matsu'ura, 1988) to demonstrate this permanent surface deformation. However, their findings suggested that long-term deformation around the subduction zone could be approximated as steady motion, and they concluded that the formation of the Numa terraces was not directly related to the Kanto earthquakes, except for Numa IV. Noda et al. (2018) proposed an explanatory model for the current elevation distributions of the Numa terraces by combining steady uplift and sea level fluctuations, a concept often applied to late-Pleistocene marine terraces. This model hypothesized that the Numa terraces might have a reversal formation age (i.e., a higher terrace is younger than a lower terrace) at certain locations. However, subsequent geological studies (Komori et al., 2020; 2021) did not find evidence to support such a feature in the Numa terraces.

In addition, previous studies have highlighted several discrepancies between existing models and geological observations of the Numa terraces. One notable inconsistency lies in the concentrated distribution of permanent uplift caused by plate subduction. In conventional crustal deformation models introduced later, the characteristic wavelength of deformation is typically comparable to plate thickness, extending broadly up to 100 km from the trench axis. However, our previous geomorphological study revealed a steep decrease in elevation within 10 to 20 km distance (Komori et al., 2020). Such feature is possibly seen in a place where upper plate faulting occurs (e.g., Clark et al., 2017), but no evidence of active inland fault is confirmed around this area. Furthermore, the feature of Numa terraces where the relative elevations do not correspond proportionally to their formation intervals (Komori et al., 2021) serves as another example of how

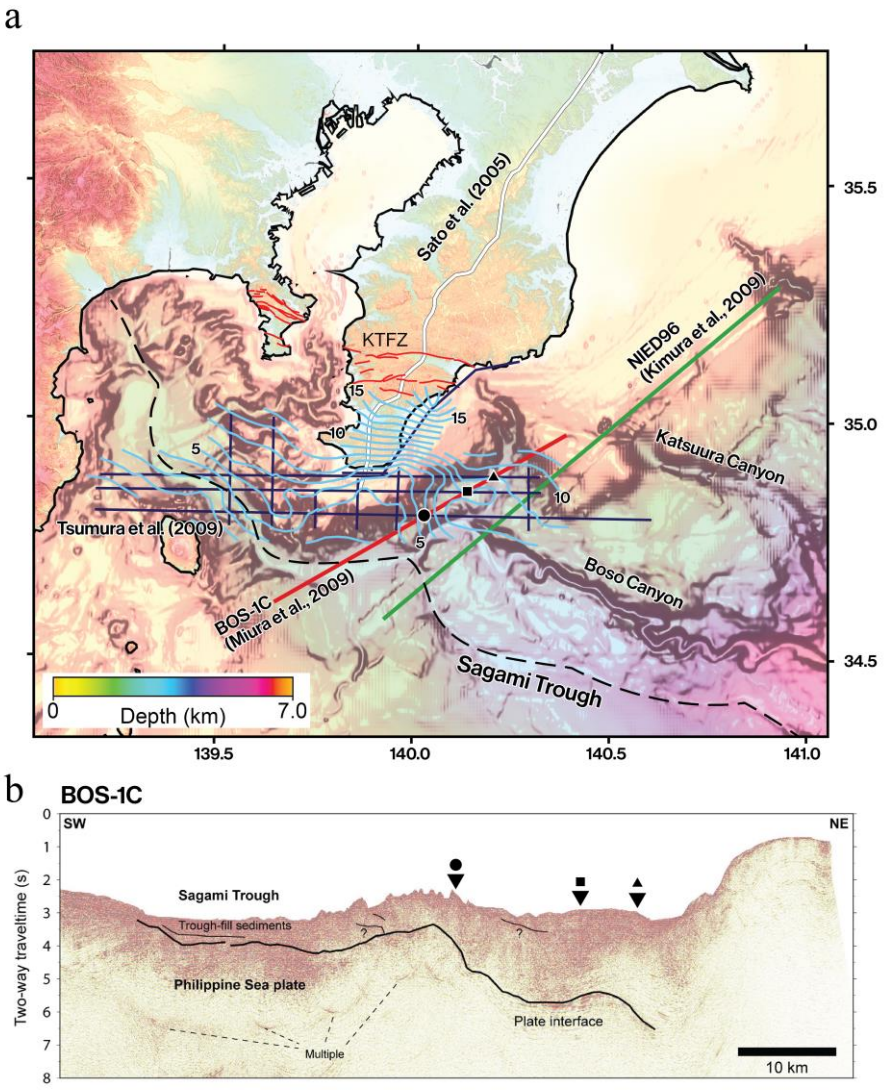

Figure 2. (a) Bathymetry map around the survey region and the profile lines of the previous reflection surveys (Sato et al., 2005; Kimura et al., 2009; Miura et al., 2009; Tsumura et al., 2009). The blue contour lines indicate the estimated depth of upper PHS by Tsumura et al. (2009), where the dark-blue straight lines are the survey profiles. The red lines indicate the inland active faults, where KTFZ stands for Kamogawa-teichi fault zone. (b) Post stack time migrated reflection image of the BOS-1C profile (Miura et al., 2009). Solid black line is our interpretation of the plate interface. Triangles indicate the positions of intersection with the survey lines of Tsumura et al. (2009).

conventional crustal deformation models fail explain the formation history, although this issue is not examined in this study. These contradictions suggest that a more fundamental understanding of crustal deformations is necessary for evaluating past earthquake histories.

This study aims to explore the relationship between permanent uplift, namely the accumulated deformation resulting from multiple earthquake sequences, and plate interface geometry. Previous reflection surveys have extensively investigated the tectonic structure around the Sagami Trough subduction zone and the upper interface geometry of the PHS. Figure 2a illustrates the profiles

from these earlier surveys (Sato et al., 2005; Kimura et al., 2009; Miura et al., 2009; Tsumura et al., 2009). Tsumura et al. (2009) conducted surveys in the nearest shore region to our study area (Figure 2a) and reported the presence of a subducted seamount. Furthermore, Miura et al. (2009) obtained a cross-section in the southeast offshore Boso (Figure 2b) that intersects multiple survey lines from Tsumura et al. (2009). A comparison of these cross-sections in the migrated time sections (see Figure 7 in Tsumura et al. (2009)) reveals comparable positions of the reflectors at the cross points. As a result, these two independent surveys strongly suggest the existence of an irregular geometry, possibly a subducted seamount, beneath the southernmost part of the Boso Peninsula. The tectonics in this subduction zone (Figure 1a) suggests that this subducted seamount is possibly a part of the Izu-Ogasawara Island Arc.

In geological studies conducted in other regions, upper plate faults branching from the main thrust have been identified as potential causes of permanent deformations around subduction zones (Plafker et al., 1969; Litchfield et al., 2020). In the surrounding region of this study area, there is no clear evidence of significant activity of intraplate faults in the upper plate. Approximately 20 km north of the study area, in the central part of the Boso Peninsula, an active fault zone (Kamogawa-teichi fault zone) is recognized (Nakajima et al., 1981). However, geological records of recent activities in the late Quaternary are not evident in this fault zone (Komatsubara, 2017). In the offshore region, Kimura et al. (2009) identified several splay faults branching from the main thrust. However, the branching faults in the shallower part, which likely form Boso Canyon at the seafloor, do not connect to other reflection survey results in the nearshore (Miura et al., 2009; Tsumura et al., 2009). It is possible that this branch fault has merged with the main thrust, where Boso Canyon meets the Sagami Trough. Another branching fault in the northeast, potentially exposed as Katsuura Canyon, appears to connect to the Kamogawa-teichi fault zone based on the seafloor topography (Kimura et al., 2009). Consequently, for the purpose of our modeling work, we assume that upper plate faulting does not significantly contribute to the crustal deformation in the region and that coseismic deformation is due to subduction interface earthquakes.

3 Subducting Plate Models

The crustal deformation models accompanying plate subduction have been proposed by various modeling studies. However, it is challenging to find an ideal model that explains all phenomena around subduction zones. Instead, these models have been developed with different scales focusing on specific phenomena. Because the target phenomena range from momentary earthquake events to long-term deformation leading to island-arc formation, we must choose the most appropriate model depending on the purpose.

This study aims to investigate the deformation resulting from a repetition of interseismic coupling and coseismic ruptures. Each co- and interseismic deformation depends on the range of coupling patches and slip amount. Hence, even with highly simplified first-order approximated models, such as back-slip models, the expected errors due to fault geometry may result within a negligible range. However, when considering the cumulative effect of these deformations over time, the differences in assumptions regarding how a plate subducts become significant. Therefore, we compared four subduction models, including three existing models and one newly developed model, while paying attention to the irregularity on the plate interface (Figure 3). In this section, we first review the settings and characteristics of the subduction models used in previous studies.

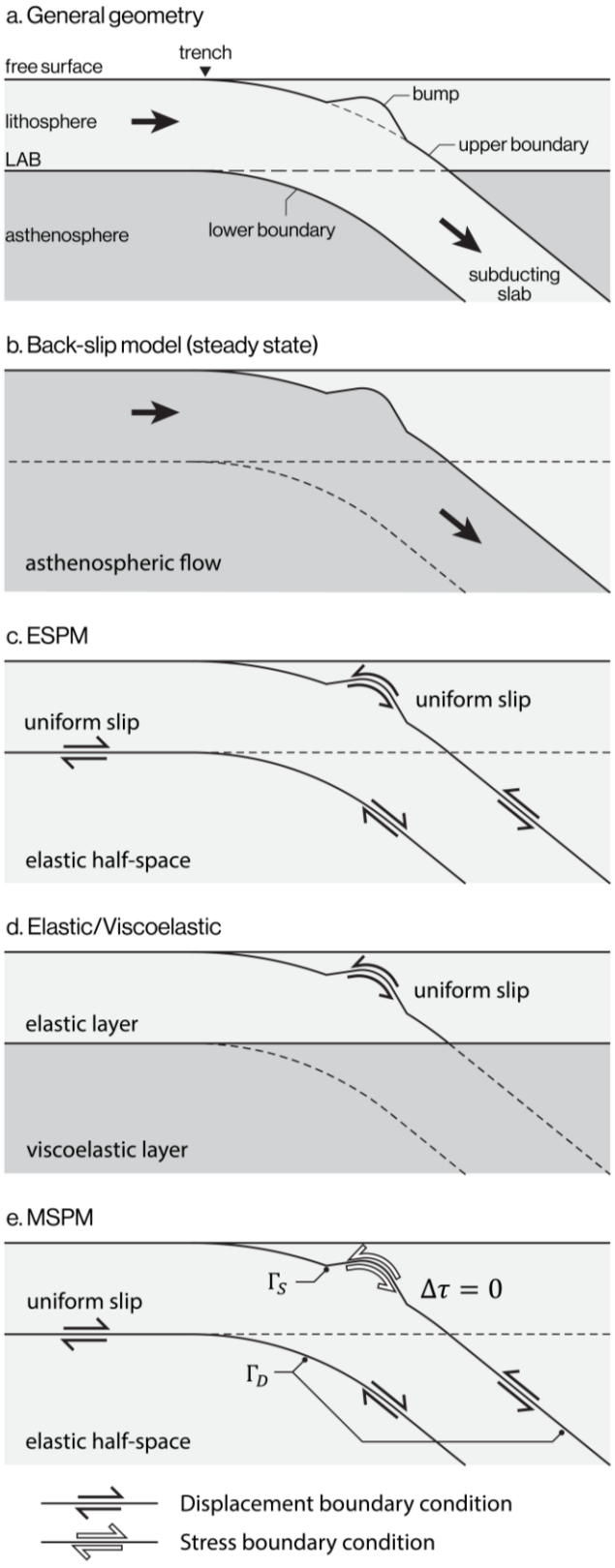

Figure 3. Schematic illustration of subduction models. (a) General geometrical setting of plate subduction. (b) Schematic representation of the imposed steady state assessed from the back-slip model, following the interpretation by Kanda and Simons (2010). (c) Slip configuration for the steady state of ESPM (Kanda and Simons, 2010). Uniform slip is imposed on the entire plate interfaces (double arrows). (d) Schematic structure illustration of the elastic/viscoelastic model. Uniform slip is imposed on the plate interface above the LAB. (e) Boundary conditions of MSPM. Black solid arrows and white arrows indicate the interfaces where uniform slip is imposed (Γ_D: area of displacement boundary condition) and no shear stress change occurs (Γ_S :area of stress boundary condition), respectively.

3.1 Back-slip Model

The back-slip model is the simplest approximation for subduction zones, first proposed by Savage (1983), that explains the strain accumulation during the interseismic period by assuming a back-slip solution due to the plate interface coupling that is given to entirely compensate the steady motion of the plate subduction (forward slip on the plate interface). This model is widely used because it only requires information on the slip deficit, the amount of back-slip, on the coupling zone, rather than constraining the slips on decoupled zone across a large part of plate interface.

However, the back-slip model exhibits a critical weakness. It assumes that steady slip along the plate boundary does not induce deformation within the upper crust, which is actually a very strong assumption. According to Kanda and Simons (2010), the back-slip model corresponds to assuming a viscously deformable subducting plate, and therefore no permanent deformation of the upper plate is produced under the steady state beyond the perturbation of the earthquake cycles, meaning the recurrence of the stress build-up and seismic slip. Figure 3b schematically illustrates this imposed steady state, where no deformation occurs within upper plate, and ignored the elastic property or complex asthenospheric flow beneath the plate interface. This model is a first-order approximation suitable only when the influence of forward slip on the entire plate interface is negligibly small. Theoretical analyses demonstrate that such a condition is attained only at a limit of flat interface geometry (or zero curvature) and uniform slip distribution (or zero slip gradient) (Romanet et al., 2020). Because the subduction interface is inevitably curved, the effect of the steady forward slip is accumulated in nature, contradicting the assumption of the back-slip model as pointed out by Matsu'ura and Sato (1989). Therefore, while it is applicable for problems like kinematic inversion of interseismic coupling, it cannot be used to model the long-term permanent deformations over multiple earthquake cycles.

3.2 Elastic Subducting Plate Model

Kanda and Simons (2010; 2012) proposed a subduction model in an elastic half space to overcome the problems with the back-slip model in treating the long-term deformation (Figure 3c). This model, elastic subducting plate model (ESPM), assumes steady slips on the upper and lower interfaces of the subducting plate. ESPM considers the long-term effect of the steady forward slip, which was neglected in the back-slip model. Further, the imposed lower interface introduced the elasticity of the plate and the asthenospheric viscoelasticity with 2D and 3D structures. As a result of bending of the subducting plate, ESPM produces the long-term permanent vertical deformations on the surface with steady subduction (forward slip). Kanda and Simons (2010) explained that this deformation is caused by the strain accumulation within the subducting plate and will remain unless the flexural stresses are released by inelastic behavior.

ESPM is an advanced subduction model that accounts for long-term permanent deformation resulting from steady forward slip, a factor overlooked in the back-slip model. However, one of the boundary conditions employed in ESPM, namely the uniform slip amount on the entire plate boundary, might become a strong assumption depending on the geometry of subduction zones. In other words, there is no mechanical validation for the assumption that slip amount becomes uniform over time. For example, recent modeling studies of earthquake events have frequently utilized dynamic rupture simulations driven by stress drops rather than kinematic slips. These simulations have revealed that the resulting slip amount is markedly sensitive to fault alignment, even under the same initial stress conditions (e.g., Ando and Kaneko, 2018). Consequently, in long-term deformation scenarios, the slip amount is also likely influenced by local irregularities in

interface geometry, even when the same stress conditions are applied due to the large-scale configuration of subduction zones. The back-slip model targets a snapshot behavior during earthquake cycles and thus can disregard the inhomogeneity accumulated over a long period. In contrast, if the model considers a longer timescale involving multiple earthquake cycles, it should account for the non-uniform distribution of accumulated slip on the plate interface.

3.3 Multilayered Elastic/Viscoelastic Half-space Model

Besides these kinematic models that assumes an elastic half-space, crustal deformation accompanying plate subduction has also been modeled using elastic/viscoelastic layered models (Matsu'ura and Sato, 1989) (Figure 3d). This model has an advantage over ESPM in the treatment of the transient behavior of the bulk viscoelasticity due to the direct Maxwellian modeling of the asthenospheric viscoelasticity. Since the stress in the viscoelastic asthenosphere is relaxed after the Maxwell time of the viscoelastic relaxation (Fukahata and Matsu'ura, 2016), the lower boundary of the elastic lithosphere behaves like the free surface in the steady state without the transient behavior. This property engages for the validity of the slipping lower surface imposed in ESPM to model the asthenospheric behavior. Fukahata and Matsu'ura (2016) explored the mechanism of permanent deformation resulting from steady subduction in this elastic/viscoelastic model, confirming that vertical deformation arises from the interaction between lithosphere bending due to the curvature of the plate interface and gravitational compensation. However, due to the theoretical limitation, their viscoelastic structure is horizontally layered, unable to account for the 2-D or 3-D structure of the subducting plate that can be important to model the case of the Sagami Trough with significant geometrical irregularity.

3.4 Limitations of Previous Models and needs for Updating Models

As stated above, the previous studies of ESPM and the multilayered viscoelastic models revealed the steady forward slip or the steady plate subduction with the curved plate geometry is important to generate the permanent uplift. However, these models only considered the first-order scale of the subduction interface geometry with assuming the uniform slip rate. Their major limitations arise from that they did not account for stress changes induced by local irregularities along the plate boundary like a subducting seamount seen in the Sagami Trough (Tsumura et al., 2019). The local geometrical structures can generate shorter wavelength patterns of permanent uplift and stress changes along the plate interface. Such a local stress can modify the slip distribution on the plate interface, and the non-uniform slip can further contribute to form the uplift patterns, where the uniform slip distribution cannot be premised. In this study, we aim at exploring the underlying mechanism of the permanent uplift in the Sagami Trough subduction zone by focusing on the irregular geometry of the plate interface. We keep our model simple as possible but the previously introduced assumption of the uniform slip is not presupposed. Moreover, we test whether the inferred subducting seamount can quantitatively explain the spatial distribution of the long-term vertical displacement rate recorded in the Numa terraces.

4 Model Setting

4.1 Mechanical Subducting Plate Model

Both ESPM and the elastic/viscoelastic model, described in the previous section, demonstrated permanent deformations resulting from the curvature of the plate interface. However, these models assume uniform slip distribution on the plate interfaces for steady state and neglect the other source

of elastic deformation, such as slip gradient (Romanet et al., 2020). As demonstrated in the following investigation, their assumption is approximately valid with a sufficiently smooth plate interface geometry but is not when it has an irregular geometry with large curvatures. Therefore, this study proposes a new subduction model that can simulate the spatial changes in slip distribution due to the irregular geometry on the plate interface, extended from the previous subduction models.

The new subduction model, MSPM, first considers the average movement over a long time period and applies boundary conditions as slips and stress changes on the plate interfaces. For example, subduction models focusing on extended time periods, such as thermomechanical models utilizing finite elements, often assume the plate interface as a thin, plastically weak layer (Bessat et al., 2020). This layer is qualitatively a boundary unable to sustain shear stress. Therefore, we can employ a boundary condition that the accumulated shear stress on the plate interface is negligible compared with the total slip amount.

Subsequently, we simplify earthquake sequences for convenience. Namely, by assuming a constant recurrence interval and persistent rupture regions, the stress accumulation per one co- and interseismic sequence aligns with the average value of long-term accumulation, which is negligibly small. Of course, it is widely acknowledged that actual individual earthquake ruptures exhibit wide-ranging variations, and it should be noted that this assumption is relatively strong. There is room for discussion regarding how the interseismically accumulated stress is allocated to each individual rupture. However, at this moment, we aim to evaluate the average behavior of recurrent earthquakes.

Consequently, the subduction model proposed in this study uses shear stress as the boundary condition instead of slip deficit, which is accumulated during interseismic periods and reduced to the level of the sliding frictional strength at the coseismic timing. To compute the interseismic stress accumulation, we developed the mechanical subduction model, MSPM, based on the configuration of ESPM (Figure 3e), by replacing the displacement boundary condition of the upper interface to the stress boundary condition to consider the nonuniform distribution of slip rates. The lower interface of the subducting slab remains the same with that of ESPM, applying the uniform displacement rate. In other words, this model operates as a stress drop model reproduces coseismic slips that release an equivalent amount of shear stress accumulated during interseismic periods due to external force. The advantage of this model is that the effects of the irregular plate interface geometry is introduced to determine the spatial variation of the slip rate in a physically consistent manner.

Besides, this mechanical model is similar to a concept of smoothing used in the recent geodetic inversion methods to evaluate the interseismic coupling that identify coupling patches instead of kinematic slip deficits (Johnson and Segall, 2004; Johnson and Fukuda, 2010; Herman et al., 2018; Herman and Govers, 2020; Lindsey et al., 2021). Conventional geodetic inversions employ smoothing parameters over the slip distribution to obtain steady results. However, such a constraint was not physically validated and might have overlooked the potentially seismogenic fault (Lindsey et al., 2021). The mechanical constraint inversion detects coupling patches on the plate interface and predicts physically reasonable slip distributions. The mechanical model employed in this study also can simulate each coseismic slip and interseismic deformation considering coupling patches, not only the steady state.

4.2 Model Geometry and Boundary Conditions

Using these subduction models, illustrated in Figure 3, the deformation patterns due to steady plate subduction and the recurrence of earthquakes are investigated. As previously mentioned, the behavior of each model would be influenced by irregularities at the plate interface. Hence, we explore the impacts of 3D model geometry and difference in the boundary conditions by considering several cases of plate geometries. Initially, we focused on a simple subduction geometry to compare the characteristics of the different subduction models introduced earlier. Figure 4 provides a visualization of the model geometry in this study. The geometry consists of a uniform cross-sectional profile along the trench axis, with the inclusion of a conical bump representing a subducted seamount. Additionally, the bottom interface of the slab is set parallel to the upper interface and has a thickness of H. In order to minimize the influence of model boundaries, we extended these surfaces with a sufficient length, although they are not depicted in this figure.

The geometry of the subducted seamount plays a crucial role in this investigation. To assess the model's sensitivity to stress changes and displacements, we explore the dependency on seamount geometries from an unusually tall bump with a height of 8 km and a radius of 15 km to the typical height of real seafloor seamounts not exceeding 4 km (Wessel et al., 2010). The seamount is adopted on the interface at a depth of approximately 10 km, as shown in Figures 4a and b.

In the ESPM and MSPM, we employed the elasto-static boundary element method with the triangle dislocation element (TDE) (Nikkhoo and Walter, 2015; Thompson et al., 2023) to implement the slip on the plate interfaces in a discretized manner. This method enables us to calculate displacements and stress changes within the elastic half-space based on linear convolutions of the Green's function with the slip amount assigned to each TDE. To impose the stress boundary condition, we calculated the shear stress change on the slip surface for MSPM by evaluating the stress at the center point of each TDE.

In the elastic/viscoelastic model, we employed the program developed by Hashima et al. (2008; 2014), which is based on the formulation by Fukahata and Matsu'ura (2005; 2006). This model is capable of calculating displacement due to a point source or a line source. Consequently, we employed a different meshing geometry from the ESPM and MSPM. For the simple subduction geometry, a uniform flat geometry along the y-axis using line sources is initially modeled. Subsequently, the bump geometry is simulated by incorporating point sources through the addition and subtraction of the bump and flat surfaces, as illustrated in Figure 4c. This superposition is made possible due to the linear relationship between displacement and slip amount in Fukahata and Matsu'ura's (2005; 2006) formulation. Because the slip within the asthenosphere has no effect, considering complete viscoelastic relaxation, the slip is only assigned to the upper interface above the lithosphere asthenosphere boundary (LAB).

As described above, if each earthquake is assumed to be an average behavior of multiple earthquake sequences, the residual resulting from asymmetry between inter- and coseismic deformations coincides to the long-term deformation pattern due to steady subduction. Therefore, we first examined the steady subduction model. In ESPM, we adopted the displacement boundary condition proposed by Kanda and Simons (2010) for the slip rates of the i-th element on the upper

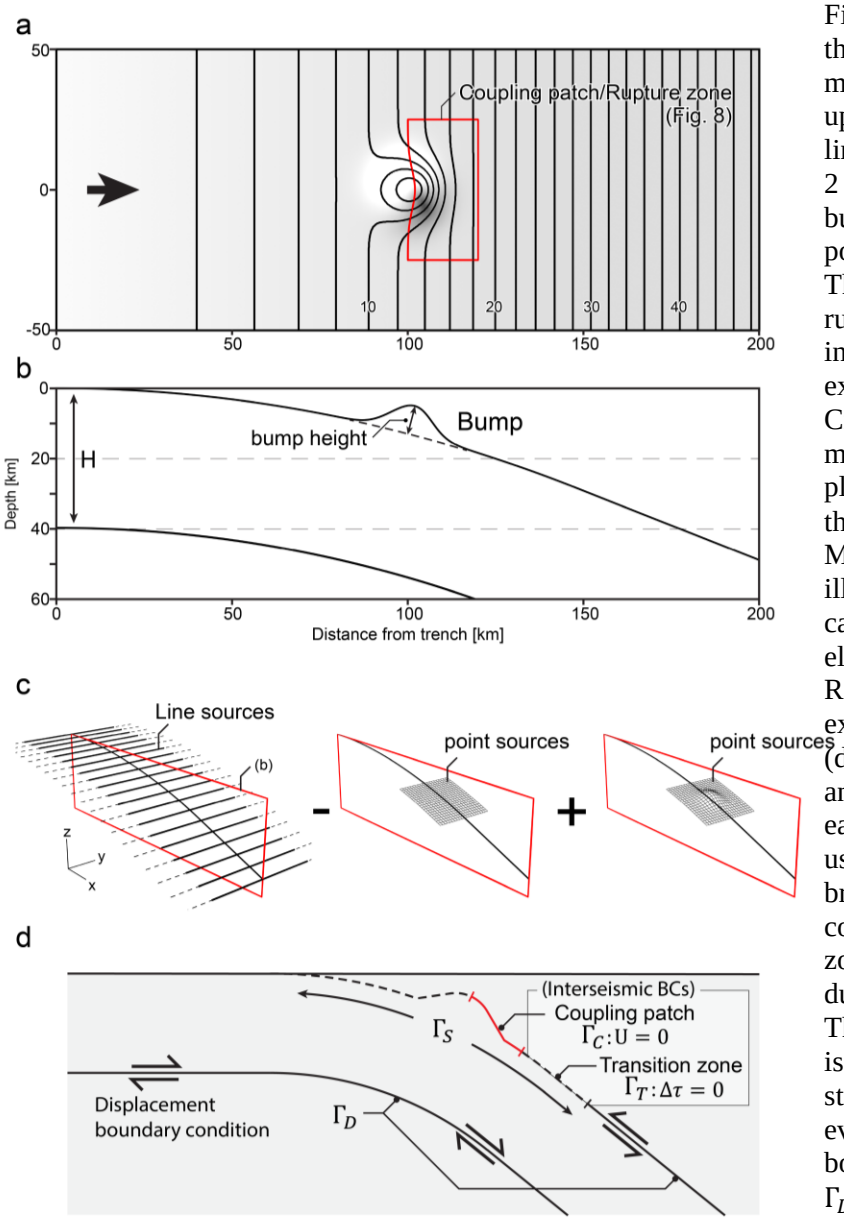

Figure 4. Geometry setting of the simple plate subduction model. (a) Plan view of the upper plate interface. The black lines indicate depth contours at 2 km interval. A conical-shaped bump with a height of 8 km is positioned at a depth of 10 km. The red rectangle indicates the rupture area and coupling patch in the earthquake sequence examination (Figure 8) (b) Cross-sectional view of the model geometry. The lower plate interface is set with a thickness H for ESPM and MSPM. (c) Schematic illustration of the superposition calculation used in the elastic/viscoelastic model. Refer to the main text for an explanation of this assumption. (d) Division of plate interfaces and boundary conditions in the earthquake sequence model using MSPM. The red and black broken lines correspond to the coupling patch and transition zone, respectively, applied during the interseismic period. The stress boundary condition is applied to the entire Γ_S during steady-state and coseismic events. The displacement boundary condition is applied to Γ_D during steady-state and the interseismic period.

and lower slab interfaces, V^i_{upper} and V^i_{lower}, respectively, where the uniform reverse and normal slips with a rate of v_{pl} (mm/year) are imposed to be $V^i_{upper} = v_{pl}$ and $V^i_{lower} = -v_{pl}$ (Figure 3c). Note that the lower interface mimics the LAB. The slip direction is parallel to the arrow depicted in Figure 4, which is perpendicular to the trench axis.

For MSPM, we consider a mixed boundary condition given by displacement and stress rates on the different areas of the plate interfaces. First, we define an area of interest on the upper interface where the stress condition is calculated. This area of stress boundary condition (AOS) is designated around the targeted geometry and coupling patches, denoted by Γ_S as depicted in Figure 4d. Outside of this AOS, Γ_D, a displacement boundary condition with a uniform slip rate is imposed on the lower interface, $V^i_{lower} = -v_{pl}$, and on the upper interface, $V^i_{upper} = v_{pl}$ when $i \notin \Gamma_S$. In

the AOS of the upper interface, we applied a stress boundary condition of the constant frictional strength uniformly, $\Delta\tau_S^i = 0$ when $i \in \Gamma_S$ (Figure 3e); accordingly, the slip rate distribution in the AOS can be linearly determined by the steady slip rate v_{pl}. The relationship between the vector representing the shear stress change $\Delta\tau_S$ in the AOS and the slip U_S ($= U^i, i \in \Gamma_S$) and U_D ($= U^i, i \notin \Gamma_S$) on the inside and outside the AOS, respectively, are described as

$$\Delta\tau_S = G_{SS}U_S + G_{SD}U_D \quad (1)$$

Where G_{SS} and G_{SD} are the matrices representing the Green's functions calculated using Thompson et al.'s (2023) code. The temporal differentiation of both side of the equations simply gives the representation for the stress rate $d\Delta\tau^i/dt$ and the slip rate V^i $\left(= dU^i/dt\right)$ with the time-independent Green's function, G. From the given boundary condition of the constant shear stress, the stress boundary condition is reduced to $d\Delta\tau_S^i/dt = 0$. Thus, the slip rate distribution on the shallower plate interface under the boundary conditions is linearly given by

$$V_S = -(G_{SS}^t G_{SS})^{-1} G_{SS}^t G_{SD} V_D, \quad (2)$$

where t denotes the transpose operation, and the indices denoting the number of elements are omitted for a simple presentation. For calculation stability and reduction, we simplified the slip direction and the calculation of shear stress change by considering only the direction parallel to the subduction direction, regarding that the trench parallel component slip is negligible in a relatively simpler geometry. For a more complex geometry, such as including branching fault, the relaxation of this assumption would be needed.

In the elastic/viscoelastic model, we simulated the steady subduction by adopting the configuration used in previous studies (Fukahata and Matsu'ura, 2016). The computation is conducted using the viscoelastic boundary element method developed by Hashima et al. (2008; 2014). The steady state is approximated by considering the situation where viscoelastic relaxation is completed. Consequently, we obtain the steady displacement and stress changes by applying uniform slip to the entire upper plate interface to be $V_{upper}^i = v_{pl}$ above the LAB at $t = 0$, after enough time with zero rigidity in the asthenosphere, following the setting in Fukahata and Matsu'ura (2016).

The structural parameters are given as shown in Table 1. In ESPM and MSPM, the structural parameters in lithosphere are applied to the entire half-space.

4.3 Earthquake Sequence Simulation

In addition to steady subduction, this study also explores an earthquake sequence using the same subduction models. The geometry of the rupture region where uniform coseismic slip occurs (in ESPM and the elastic/viscoelastic model) and the coupling patch (in MSPM) are defined according to the configuration depicted in Figure 4a. We investigated how surface deformation patterns change throughout the interseismic period depending on the subduction models.

The implementation of the earthquake sequence model using ESPM is straightforward. The interseismic coupling zone, namely coseismic rupture zone, is set initially on the upper plate interface, and uniform interseismic slip rate is assigned to the entire plate boundary, excluding this coupling zone. An earthquake sequence is represented by a coseismic slip that releases the accumulated slip deficit in the coupling zone.

In the elastic/viscoelastic model, coseismic slip is applied to designated rupture region at $t = 0$, and the post-seismic deformation or viscoelastic relaxation is taken into account. Displacements caused by slip outside the rupture region can be treated as steady deformations with a fully relaxed asthenosphere model, like the steady subduction model.

In the earthquake sequence model using MSPM, the AOS, Γ_S, is further divided into two parts; the coupling patch, Γ_C, and the transition zone, Γ_T (Figure 4d). In the interseismic period, the slip on the coupling patch is not allowed, i.e., $V_C^i = 0$ when $i \in \Gamma_C$, and the shear stress $\Delta\tau_C$ is accumulated there. The area surrounding the coupling patch steadily slip at a prescribed sliding frictional strength, $\Delta\tau_T^i = 0$ when $i \in \Gamma_T$, where the slip amount gradually increases without accumulating shear stress there. The slip rate outside the AOS is uniform, same as the steady state. Similarly in the case of steady state (equation 1), linear convolutions of the Green's function are given by

$$\Delta\tau_C = G_{CC}U_C + G_{CT}U_T + G_{CD}U_D \quad (3)$$

$$\Delta\tau_T = G_{TC}U_C + G_{TT}U_T + G_{TD}U_D \quad (4).$$

Here, when the duration of the interseismic period is given by t_{cycle}, $U_C^i\ (=0), U_D^i\ (= \pm v_{pl}t_{\mathrm{cycle}})$, and $\Delta\tau_T^i\ (=0)$ are known, and therefore U_T can be linearly calculated using equation 4. Now, for equation 3, since we already know each slip distribution, U_C, U_T, and U_D, the accumulated shear stress on the coupling patch, $\Delta\tau_C$, is calculated straightforward.

At a seismic event, the coupling patch is allowed to slip to release the accumulated shear stress during the interseismic period, $\Delta\tau_C$, while the shear stress change outside the coupling patch persists zero, $\Delta\tau_t^i = 0$ when $i \in \Gamma_T$. Combining the coupling patch and the transition zone into the AOS again, the stress drop vector for a seismic event $\Delta\tau_S$ is given by $\Delta\tau_S^i = \Delta\tau_C^i$ when $i \in \Gamma_C$ and $\Delta\tau_S^i = 0$ when $i \in \Gamma_T$. Using the linear convolution of equation 1 and that the slip amount outside the AOS at a seismic event is zero, $U_D^i = 0$, the coseismic stress distribution is calculated by $U_S = (G_{SS}^{\mathrm{t}}G_{SS})^{-1}G_{SS}^{\mathrm{t}}\Delta\tau_S$.

4.4 Crustal Deformation Simulation of the Sagami Trough

This study further investigates the crustal deformation distribution around the Sagami Trough, simulating the observed plate interface geometry obtained from seismic surveys. The upper interface geometry of PHS is created, as depicted in Figure 5, based on the observation results presented in Figure 2. This simulation employs MSPM with the lower plate interface set to a thickness of $H = 40$ km. As the focus of this investigation is the effect of the subducted seamount identified by Tsumura et al. (2009), the AOS is limited to the shallow part illustrated in Figure 5. The displacement outside this region is constrained to be a uniform slip parallel to the subduction direction, N30W, indicated by the arrow. Moreover, we simulate the coseismic and interseismic deformations around the Sagami Trough by implementing a coupling patch, as depicted in Figure 5. The same method as in the previous section is applied to simulate earthquake sequences. This allows us to evaluate the temporal deformation resulting from an earthquake sequence. The structural parameters used in this simulation are the same as those used in the simple geometry model (Table 1).

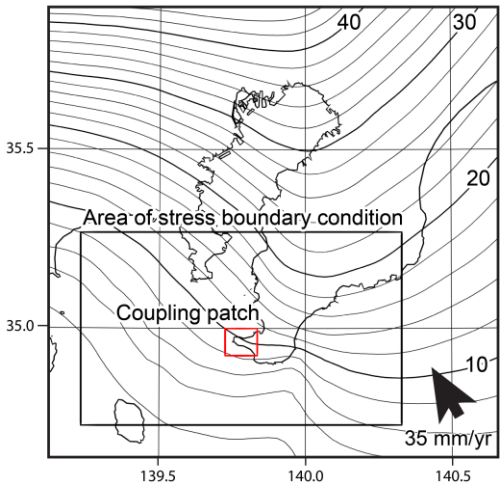

Figure 5. Geometry setting of the model simulation for the Sagami Trough subduction zone. The contour is the depth distribution of the upper plate interface of PHS, referring to Hashimoto et al. (2004), Hirose et al. (2008), and Tsumura et al. (2009). The black rectangle indicates the AOS, including a coupling patch for the earthquake sequence model, denoted by the red rectangle. Outside of the AOS is steady slip area, where uniform slip is imposed in the direction indicated by the arrow.

Table 1. Structural model

	h (km)	μ (GPa)	K (GPa)	η (Pa·s)	ρ (kg/m3)
Lithosphere	-	30	50	-	3000
Asthenosphere	40	50	90	10^{19}	3400

5 Result

5.1 Internal Stress Changes around the Interplate Bump

Figure 6 presents the simulated distributions of deformation and stress change resulting from steady subduction using different subduction models. The top, middle and bottom panels represent the results obtained with ESPM (Kanda and Simons, 2010), the elastic/viscoelastic two layered model (Fukahata and Matsu'ura, 2005; 2006), and MSPM (developed by this study), respectively. In these figures, the displacement and the von-Mises stress change in the x-z plane are depicted using arrows and color maps, respectively. In the elastic/viscoelastic model (Figures 6c and d), the displacement is shown relative to the values obtained at a distant point from the subduction axis in the hanging wall side. The arrows in the outer part of the subducting slab (bluish color) are exaggerated by a factor of ten. Figures 6a, c, and e provide an overall view of the results, while Figures 6b, d, and f offer closer views around the bump region. Figure 6g shows the slip amount distribution on the fault using MSPM. In the case of ESPM and elastic/viscoelastic model, the slip amounts are identical to the unit slip rate v_{pl} on the entire fault.

We can interpret the variations in the internal stress changes resulting from different employed models. The stress changes resulting from steady subduction with a smoother plate interface, as discussed by Kanda and Simons (2010) and Fukahata and Matsu'ura (2016), are insignificant compared to the stress changes induced by the bump geometry introduced in this study. Figure 6 clearly demonstrates that noticeable stress changes occur around the bump geometry in all cases. Note that in the elastic/viscoelastic model (Figures 6c and d), singularity values are observed around the plate interface because this model employs point sources. The stress concentration observed around the bump using ESPM is significantly larger than that using MSPM.

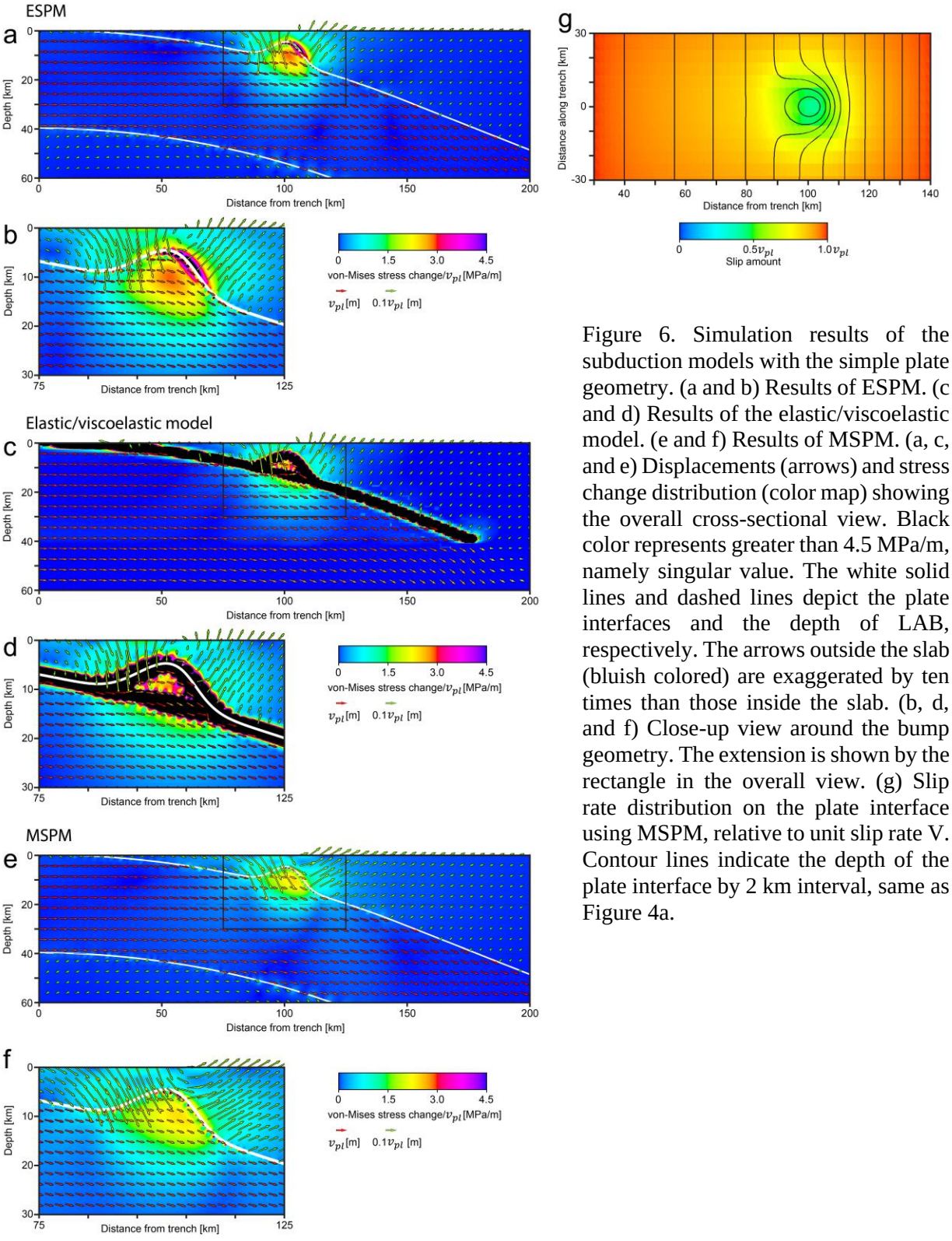

Figure 6. Simulation results of the subduction models with the simple plate geometry. (a and b) Results of ESPM. (c and d) Results of the elastic/viscoelastic model. (e and f) Results of MSPM. (a, c, and e) Displacements (arrows) and stress change distribution (color map) showing the overall cross-sectional view. Black color represents greater than 4.5 MPa/m, namely singular value. The white solid lines and dashed lines depict the plate interfaces and the depth of LAB, respectively. The arrows outside the slab (bluish colored) are exaggerated by ten times than those inside the slab. (b, d, and f) Close-up view around the bump geometry. The extension is shown by the rectangle in the overall view. (g) Slip rate distribution on the plate interface using MSPM, relative to unit slip rate V. Contour lines indicate the depth of the plate interface by 2 km interval, same as Figure 4a.

Figure 6g, showing the slip rate distribution around the subducted seamount calculated by MSPM, indicates that the slip rate is lower in the vicinity of the seamount compared to the surrounding areas. If a uniform slip rate V was applied in the entire area here, the result is identical to ESPM. Hence, the essential difference between ESPM and MSPM is in this slip rate distribution.

5.2 Patterns of Surface Displacements

Figure 7a presents the permanent vertical surface displacements with each subduction model, relative to the unit slip rate v_{pl}. If an averaged earthquake sequence is assumed, these patterns coincide the residual resulting from asymmetry between inter- and coseismic deformations. Specifically, permanent uplift is observed above the subduction side of the seamount (leading flank), while subsidence occurs above its trench axis side (trailing flank). Although overall features are comparable to each other, differences can be seen at the uplift peak. The peak uplift in MSPM is more gradual and smaller than that in ESPM. The difference between ESPM and MSPM, including displacements and stress changes, can be attributed to variations in slip distributions on

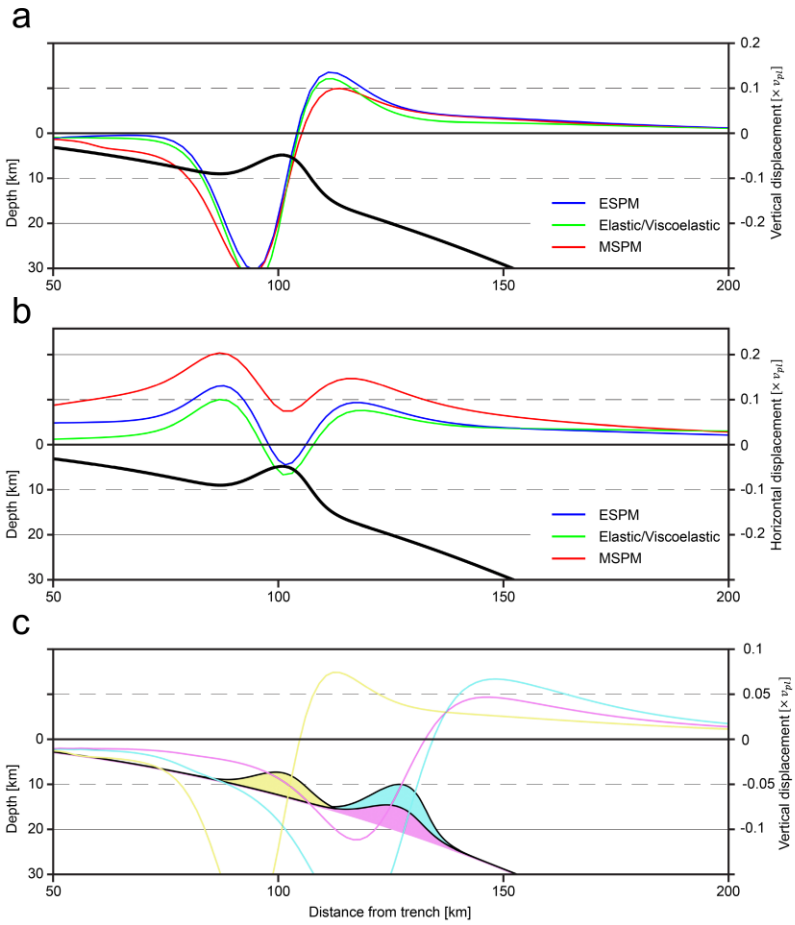

Figure 7. (a and b) Vertical and horizontal displacement distribution in each model. These results correspond to the arrows on the surface depicted in Figures 6 a, c, and e. Positive value indicates movements towards the subduction direction in (b). (c) Vertical displacement distributions with different bump geometries. The line colours correspond to the geometries of subducted seamounts. MSPM model was used for these simulations.

the fault around the bump geometry (Figure 6g). The slip becomes smaller when the bump exists, leading to the smaller vertical displacement; in other words, ESPM means to impose unrealistically large slip along the bump. The horizontal component of the displacements in MSPM shows a bulk movement towards the subduction direction, which reflects the dragging due to the stacked bump (Figure 7b). Although the back-slip model results are not presented in this figure, it is worth mentioning that in the back-slip model, the displacements and stress change in the hanging wall consistently remain zero, regardless of the plate interface geometry, resulting from the subducting slab exhibits smooth deformation attributed to asthenospheric flow, as described in Kanda and Simons (2010).

As a result, the previous subduction models that assign uniform slip distribution along the entire plate interface for steady state may not accurately capture the displacement distribution and stress concentration around the bump geometry because of the enforced slip distribution ignoring the slip direction. In contrast, MSPM effectively represents the movement of the subducted bump stacking towards the hanging wall (Figure 7b), implying a dragging movement, and helps alleviate stress concentration around the bump.

The short-wavelength permanent vertical deformation, which was not effectively explained with the conventional model setting, can be qualitatively explained by all the models depicted in Figure 7a. While the deformation patterns are similar between the models, it is important to note that the differences among the models become larger for rougher and more irregular geometries, which could impact the analysis aimed to understand the fault geometry effect on the geodetic and geological observations.

Figure 7c depicts the surface deformation using MSPM with different subducted bump geometries. The yellow, magenta, and cyan lines represent the permanent vertical deformations associated with shallow short, deep short, and deep tall bumps, respectively, as indicated in the bottom part of the figure. It can be observed that shallower and larger bump geometries result in greater amounts of permanent displacement. Furthermore, in the case of the shallower bump, the short-wavelength deformation is more pronounced. It is important to note that the estimation of subducted seamount geometry is challenging and subject to uncertainties, with potential errors of a few kilometers. This analysis underscores the potential impact of different assumptions regarding the bump geometry, leading to different expectations for surface deformation.

Figure 8 displays the results of the earthquake sequence simulations. This earthquake sequence assumes that the rupture occurs over the same rupture pattern with a constant interval t_{cycle} in each model. The results in Figure 8 are the vertical displacements relative to the total subduction amount $v_{pl}t_{cycle}$. The red and blue lines represent the coseismic and interseismic vertical deformation patterns, respectively. The green line represents the total vertical deformation pattern, which is identical to the result shown in Figure 6g. The yellow lines are the snapshots at every 1/5 t_{cycle}. In the deformation pattern at $t = t_{cycle}$, namely at the completion of an earthquake sequence, the shaded portion corresponds to 'residual uplift,' where uplifts occur in both the coseismic and long-term average deformations. This residual uplift leads to the formation of marine terraces that remain above sea level. It should be noted that the specific patterns of coseismic and interseismic deformation are influenced by the position and size of the rupture area. Therefore, Figure 8 serves as an example illustrating possible deformation patterns that can arise from an earthquake sequence.

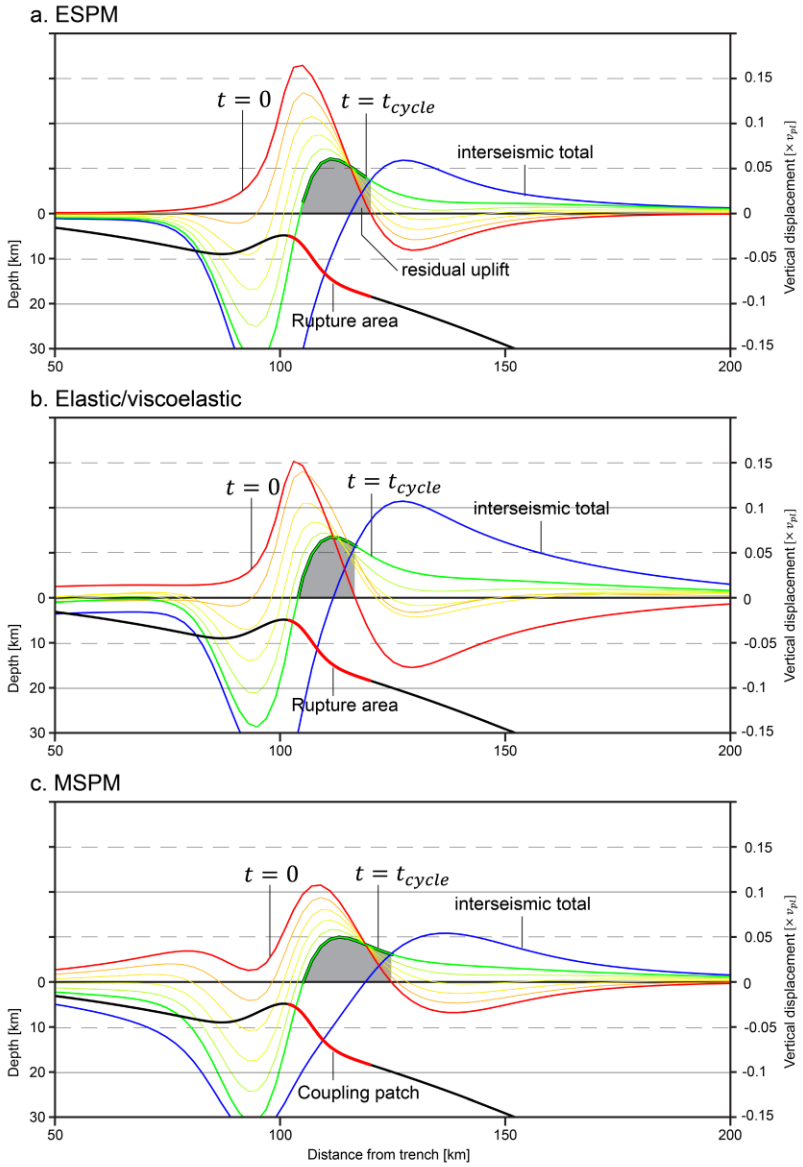

Figure 8. Transition of vertical displacements resulting from the earthquake sequence models. The red portion of the plate interface geometry indicates range pf the rupture area (ESPM and Elastic/viscoelastic model) and coupling patch (MSPM), as shown in Figure 4. Red lines present the coseismic vertical deformation at $t = 0$ and transits into the terminal deformation pattern at $t = t_{cycle}$ depicted by the green lines. Yellow lines represent the snapshots of this transition at every 1/5 t_{cycle}. The differences between red and green lines are interseismic total deformation, which is depicted by the blue lines. The shaded portions of the green lines indicate the residual uplift, where uplifts are observed both in coseismic and terminal deformation patterns.

598

599 ### 5.3 Simulated Deformation Distribution of the Sagami Trough

600 Figure 9 depicts the surface vertical deformation pattern using the geometry of the Sagami
601 Trough subduction zone (Figure 5). In Figure 9a, the vertical deformation is shown for steady
602 subduction (long-term average) using MSPM. Figure 9b illustrates the modeled coseismic vertical

deformation. The coseismic rupture is simulated by setting a coupling patch, shown as the red rectangle in Figure 9b, that represents the southeastern coupling patch suggested by the results of geodetic inversion (Sagiya, 2004; Noda et al., 2013), which is assumed as the main rupture portion of the 1703 Genroku earthquake. The deformation amounts are expressed relative to the convergence rate v_{pl} for the long-term deformation and total subduction amount $v_{pl}t_{cycle}$ during the interseismic period for the coseismic deformation, respectively. Figure 9c shows the comparison between the simulated vertical displacement rate, as shown in Figure 9a, and the observed elevation distribution of the highest paleo-shoreline, which indicates the sea level at the Holocene highstand, compiled by Shishikura (2014). The observation points for the highest paleo-shoreline are depicted in Figure 9a by red circles. For comparison, the amplitude of the simulated vertical displacement rate is adjusted by assuming the convergence rate v_{pl} and the age of the highest paleo-shoreline to be 35 mm/year (Seno et al., 1993) and 7,000 BP, respectively. Moreover, considering the sea-level change after the Holocene highstand, the vertical displacement is shifted by 5 meters.

As shown in Figure 9c, when considering the highest paleo-shoreline as indicative of long-term deformation distribution, there is notable agreement between the observations and simulation results on the eastern coast. In particular, the sharp decline in uplift rate from the southernmost tip

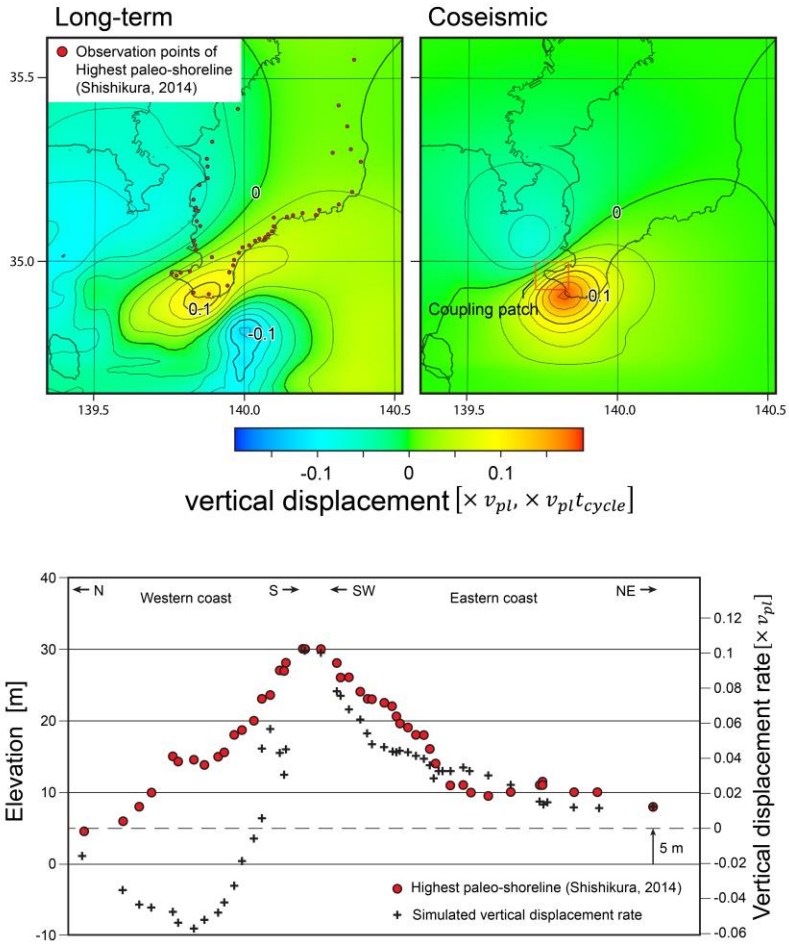

Figure 9. Simulated deformation distributions using MSPM with the model geometry of the Sagami Trough subduction zone. (a) Vertical displacement rate distribution with the steady-state assumption. (b) Coseismic vertical deformation distribution with the coupling patch representing the 1703 event, depicted by the red rectangle. (c) Comparison between the observed elevation distribution of the highest Holocene paleo-shoreline (Shishikura, 2014) and simulated vertical displacement rate. Observation points are displayed in (a). The amplitude of vertical displacement is calibrated assuming that the convergence rate and the age of the highest Holocene sea level are 35 mm/year and 7,000 BP. The vertical displacement is shifted by 5 meters reflecting the Holocene highstand.

towards the northeast, where the highest uplift rate closely corresponds to the observed data. However, on the western coast, while the deformation rate similarly decreases towards the north, it exhibits a long-term subsidence trend, contrary to the observed pattern. Figure 9b shows the coseismic vertical deformation amount at the southernmost tip of the Boso Peninsula, which is approximately 0.18 $v_{pl}t_{cycle}$. Assuming that the rupture of this patch occurs every 2,000 years (Shishikura, 2014), the estimated coseismic uplift is approximately 5.4 m. This estimate is comparable to the observation of the marine terraces.

Following the simplification assumption of earthquake sequences, as proposed in the examination show in Figure 8, the residual deformation pattern after an earthquake sequence, i.e., relative height of terraces, matches the long-term deformation pattern, as shown in Figure 9a. However, as discussed in previous papers (Komori et al., 2020; 2021), the formation pattern of marine terraces in this region is complex and cannot be explained solely by a simple periodic rupture. The results presented in this study demonstrate the effects of subducted seamounts and the capability of MSPM to explain the rupture and deformation history along the subduction zone.

6 Discussion

6.1 Optimal Subduction Model for Irregular Plate Interface

The uplift accumulation observed around subduction zones has been the subject of extensive research due to geological observations, such as marine terraces. However, previous kinematic models primarily assumed a smooth plate boundary interface and attributed permanent uplift to deformation within the subducted slab or asthenospheric flow. It has become evident through observation, including the sand-box experiments (Dominguez et al. 1998; 2000) and the coastal landform (Kodaira et al., 2000; Gardner et al., 2001), that irregularities in the plate interface strongly influence permanent deformation. Additionally, the impact of fault curvature on the deformation was emphasized in previous mechanical investigations (Romanet et al., 2020). Thus, it is crucial to incorporate the effects of these irregularities when evaluating crustal deformation resulting from plate subduction. However, previous kinematic models often employed a boundary condition imposing uniform slip across the entire plate interface, which leads to unrealistic mass flow in the elastic medium along curved slip surfaces when local irregular curvature exists. To address this limitation, we have developed a new mechanical model capable of simulating plate subduction with irregular bump-shaped interfaces and compared its performance to the previous models.

The stress boundary condition in this study's model, MSPM, with the constant sliding friction is physically more reasonable than imposing a uniform slip on the entire fault. As depicted in Figure 6, the stress accumulations resulting from steady subduction around the subducted bump exhibit significant differences between MSPM and the previous models, ESPM and the elastic/viscoelastic model. The previous models show large stress accumulation in both the upper and lower sides of the subducted bump, which is caused by the bending of dislocation surface in the elastic medium. In contrast, MSPM simulates gradually decreasing displacements within the subducted bump (Figure 6f). Qualitatively, this deformation resembles the dragging of the stacked bump. Consequently, the displacement field, which was artificially simulated by the slips on the plate interface, is expressed by the gradual shear deformation within the bump. As a result of this deformation distribution, the artificial stress concentration in the upper side of the bump was eliminated.

Despite the significant difference within the internal stress condition, the vertical deformation demonstrated a qualitatively common pattern throughout those subduction models, where permanent uplift and subsidence concentrations occur above the leading and trailing flanks of the subducted seamount, respectively. As demonstrated in Figure 7, the difference in deformation amounts between each model are significant when employing identical plate interface geometry. However, when this is applied to actual plate geometries, the observation error of plate interface depth could exceed several kilometers. Furthermore, observation values are frequently derived from geological studies, further challenging to minimize observation errors. Consequently, the imperative to differentiate these models in practice may be overshadowed by the estimation errors stemming from observational inaccuracies.

However, analyses that attribute model approximations to observation errors can lead to misunderstandings and incorrect assumptions, as they may obscure mechanical inconsistencies and force overfitting between observations and simulation results. This is why the back-slip model has been overused inappropriately in problems related to subduction zones, disregarding its first-order approximation. Of course, it should be noted that MSPM is also an approximate model, but a step-by-step process to reduce mechanical inconsistency is essential. Additionally, as demonstrated in Figure 8, mechanical boundary conditions offer advantages in simulating more realistic behaviors of coseismic slip and interseismic coupling. Therefore, for the analysis of subduction zone deformations within a timescale of 10 to 100 thousand years, where the movement of subducting bump itself can be ignored, we would recommend utilizing the model with the mechanical boundary condition.

In this study, MSPM does not incorporate viscoelastic relaxation in the asthenosphere, like ESPM where steady slip on the bottom interface of the slab is assumed to simulate asthenospheric flow. As a result, the isostatic compensation resulting from the gravitational effect, which was focused in Fukahata and Matsu'ura (2016), is not accounted for in MSPM. While this effect may have a characteristic wavelength comparable to the lithosphere thickness and could be less significant in our current interest of the local surface deformation distribution, it is still worth discussing for precise estimations, particularly in cases of extreme uplift and subsidence. Figure 6e illustrates that the elastic/viscoelastic model exhibits singular values on the slip surface, making it unsuitable for the stress boundary conditions. On the other hand, models in the elastic half-space can be used to simulate the viscoelastic effect. The condition where stress in the asthenosphere is fully relaxed after enough time can be approximated by assuming the rigidity of the asthenosphere is zero, which behaves like water, as discussed in Fukahata and Matsu'ura (2016). Thus, the permanent deformation can be modeled by incorporating boundary conditions that the stress accumulation on LAB is zero, where uniform slip is applied to in MSPM. Moreover, this configuration allows for the simulation of complex geometries in the subduction zone, unlike the elastic/viscoelastic model, which simulates a horizontally layered half-space.

6.2 Remaining Uplift after Earthquake Sequence

The relationship between marine terrace distribution and coseismic uplifts has long been paid attention. First, the primitive back-slip model fails to explain the mechanism of permanent deformation and marine terrace formation because the coseismic uplift is canceled out by interseismic subsidence. Studies conducted in other subduction zones have attempted to verify whether coseismic deformation would be completely recovered by interseismic deformation and matches the long-term deformation pattern, based on historical and geological records (Briggs et al., 2008; Wesson et al., 2015). Most of these studies have not produced observations indicating

that coseismic deformation corresponded to (reversed) interseismic deformations or the long-term deformation pattern. Consequently, the asymmetry between co- and interseismic deformations has been widely accepted from observational studies, while it is possibly attributed to upper plate faulting.

In a study by Sato et al. (2016), the recent deformation around the Sagami Trough was simulated using an elastic/viscoelastic model. It was concluded that coseismic uplifts are negligible due to subsequent interseismic subsidence, and they are considered as a 'perturbation' within the long-term steady uplift. In this study, the perturbation caused by coseismic uplifts was quantitatively evaluated using three subduction models. It was observed that if both long-term and coseismic uplifts are significant, the coseismic uplifts never return to sea level throughout earthquake sequences. This condition may occur above the leading flank of a subducted seamount.

This study examined deformations throughout each earthquake sequence. However, the earthquake sequences analyzed here (as shown in Figure 8) are based on idealized average-type earthquakes occurring over extended periods, akin to so-called characteristic earthquakes. The issue would arise when considering variations in individual earthquake ruptures and their resulting deformation patterns. Nonetheless, the consistent explanation of marine terrace formation was successfully demonstrated in at least the end-member earthquake sequences. As a result, the rebuttal to the previous argument seeking to attribute the causes of marine terrace formation to eustatic sea-level fluctuations (Noda et al., 2018) has been achieved.

Traditionally, paleoseismological studies have often estimated the magnitudes of past earthquakes and compared their similarity based on the elevation distribution of the marine terraces. However, the findings of this study suggest that the remaining terrace distribution does not directly indicate the coseismic uplift distribution. While it is possible to estimate the minimum magnitude of past earthquakes based on the extent of terrace formation, as it requires a sufficient initial uplift amount, the similarity of terrace distribution alone cannot identify the rupture region and characteristic earthquakes. Therefore, for a precise estimation of past rupture history along subduction zones, the correction of the interseismic deformation is essential, and must be based on other geological and geophysical data.

6.3 Simulation of Geological Observations

In this study, the long-term vertical deformation distribution around the Sagami Trough was evaluated using MSPM and the depth distribution of the PHS obtained from recent seismic surveys. The results showed that the long-term deformation is primarily influenced by the geometry of the plate interface because the influence of coupling patch will be declined over time. Thus, the permanent vertical deformation depicted in Figure 9a can be attributed to the subducting plate geometry shown in Figure 5. The southernmost tip of the Boso Peninsula exhibited the highest uplift rate, reaching 0.12 v_{pl}. This location corresponds to the area above the leading flank of a subducted seamount, as observed by Tsumura et al. (2009). Although there are uncertainties associated with the convergence rate and seamount geometry, this uplift rate is comparable to the long-term uplift rate estimated from the height of the Holocene highest marine terrace observed in the region (Shishikura, 2014) (Figure 9c). Additionally, the elevation distribution, which peaks at the southernmost tip, is consistent with this uplift rate. Therefore, it can be concluded that there is a considerable possibility that the long-term deformation of the Boso Peninsula is influenced by the presence of the subducted seamount.

However, the overall distribution of the permanent vertical deformation does not necessarily align with the geological observations. For instance, although the model predicts long-term

753 subsidence around the Miura Peninsula, geological evidence such as Holocene and Pleistocene
754 marine terraces suggests an uplift trend in this area (Figure 9c). This subsidence trend in this model
755 possibly arises from the curvature of the model geometry in the northwestern part. The accuracy
756 of the depth distribution, particularly in the deeper part of the subduction zone, is highly uncertain
757 and may contribute to the discrepancies observed in the long-term deformation distribution.
758 Additionally, the western end of the Sagami Trough exhibits a complex plate boundary due to the
759 collision of the Izu Peninsula, which deviates from a simple steady subduction scenario
760 (Hashimoto and Terakawa, 2018). This collision may introduce complexities that cannot be
761 captured by the subduction models used in this study. Consequently, the crustal deformation
762 around the Izu Peninsula may not be accurately simulated using the subduction models employed
763 here. As a result, the coverage of this study is currently limited to the southern part of the Boso
764 Peninsula, where the influence of the collision is smaller and the resolution of the depth distribution
765 of the subducting plate is higher.
766 Figure 9b presents the distribution of coseismic vertical deformation when a coupling patch,
767 represented by the red rectangle, is considered. The uplift observed at the southernmost tip of the
768 Boso Peninsula is approximately 0.18 $v_{pl}t_{cycle}$. Assuming a rupture interval of 2,000 years for
769 this specific coupling patch, the estimated coseismic uplift is consistent with the observed
770 elevation of the Genroku terrace, where the maximum elevation is approximately 7 m. It is
771 important to note that the chosen rupture recurrence in this analysis is a subjective forward model
772 and may not represent the actual recurrence pattern. However, this result suggests that the MSPM
773 model has the potential to simulate realistic terrace formation, indicating its capability in capturing
774 essential aspects of the process.
775 The formation history of the Numa terraces and the rupture history of the Sagami Trough
776 require a more detailed and thorough discussion, taking into account the complexities observed in
777 previous studies (Komori et al., 2020; 2021). These studies have shown that the formation intervals
778 and relative heights of the Numa terraces are not consistent with each other, indicating a more
779 complex pattern of terrace formation. Additionally, the rupture interval of 2,000 years, based on
780 the terrace formation ages, is much longer than the typical recurrence interval for subduction
781 earthquakes. This discrepancy strongly suggests that the rupture pattern of the Sagami Trough is
782 not periodic and does not in occur the same region each time. To fully understand the rupture
783 scenario of the Kanto earthquakes and provide a comprehensive explanation for the formation
784 history, it is essential to employ a physically consistent model that considers coseismic,
785 interseismic, and long-term deformations. The MSPM used in this study is well-suited for this
786 purpose as it allows for the simulation of rupture recurrence that considers the accumulation and
787 release of stress.
788 In addition to the effects of subducted seamounts, we cannot yet eliminate other potential
789 sources of deformation within the hanging wall of subduction zones. Inelastic faulting, including
790 splay faults and upper plate faults, can occur due to the compression stress field associated with
791 plate subduction. These faulting events can contribute to the overall surface displacement field and
792 result in complex deformation patterns (e.g., Hikurangi subduction margin, as discussed in Clark
793 et al. (2017)). Analogue experiments conducted by Dominguez et al. (1998; 2000) have
794 demonstrated that strain accumulation within the hanging wall caused by seamount subduction can
795 be released through inelastic deformation.
796 Although major faults have not been identified in the Sagami Trough region based on seismic
797 surveys, several studies have suggested the possibilities of such movements (Pollitz et al., 1996).
798 In this context, model examinations and investigations into the possibility of inland faulting can

be valuable. The MSPM used in this study is a suitable tool for evaluating the stress conditions within the plates and can provide insights into the potential mechanisms and effects of inelastic faulting in the subduction zone. By considering multiple deformation sources and incorporating various geological and geophysical observations, a more comprehensive understanding of the deformation processes in the study region can be obtained.

7 Conclusion

This study examined the formation of uplifted marine terraces around subduction zones, namely residuals resulting from asymmetry between inter- and coseismic deformations, focusing on the impact of plate interface irregularities. Because existing subduction models have implicitly assumed a smooth plate interface geometry, we first discussed the mechanical behavior around a bump on a plate interface and appropriate boundary conditions for such problems. The models utilized in this study differ in their approach to simulating plate subduction. ESPM and the elastic/viscoelastic model employ a uniform slip distribution on the plate interface, while MSPM imposes the constraint that the shear stress change should be net zero. Additionally, the elastic/viscoelastic model incorporates stress relaxation within the asthenosphere using a two-layered half-space model, whereas in ESPM and MSPM, the uniform slips on the bottom interface of the slab account for this movement. To examine the behavior of these models, a simple plate interface geometry with a bump shape was considered. The results showed that all three models were capable of producing localized uplift above the leading flank of the subducted seamount. However, there were notable differences in the displacement distribution within the crust. MSPM exhibited a more gradual displacement distribution compared to ESPM and the elastic/viscoelastic model. This difference arises from the extraordinary stress concentration that occurs when enforcing uniform slip on the bump in the models. In contrast, MSPM avoids such concentration by constraining the shear stress change to zero. Based on these findings, MSPM is considered to be a suitable model for simulating plate subduction when the plate interface exhibits local irregularities, such as a subducted seamount.

The analysis of vertical deformation around the subducted seamount revealed that it can play a crucial role in the formation of coastal landform, with larger vertical deformation than previously explained by the bending of the subducting plate. The patterns of permanent surface deformation slightly differ among the models used, but these differences are less significant compared to the variation caused by the size and geometry of the subducted seamount. Although it is currently challenging to directly validate the appropriateness of the models based on geological and seismic observations, it can be inferred that the significance of the subducted seamount in the deformation process is independent of the specific subduction model employed. In other words, regardless of the model used, the presence and characteristics of the subducted seamount have a substantial impact on the resulting deformation patterns and cannot be ignored.

The formation mechanism of marine terraces has been a subject of interest in understanding the recurrence of past earthquakes. Using the basic back-slip model, the coseismic uplifts are eliminated by subsequent interseismic coupling, making it difficult to explain the formation of marine terraces. Previous modeling studies using elastic/viscoelastic layered half-space models also suggested that individual earthquake sequences cannot generate sufficient remaining uplift to form marine terraces. However, this study demonstrates that the presence of subducted seamount can contribute to the coseismic and long-term uplifts, which provides a plausible mechanism for marine terrace formation through coseismic deformation. It should be noted that the correlation between the remaining deformation (i.e., relative heights of marine terraces) and the distribution

844 coseismic uplifts may not always be straightforward. Therefore, to accurately estimate the past
845 rupture history from the present distribution of marine terraces, it is essential to carefully evaluate
846 the interseismic deformation and employ a physically consistent model of rupture recurrence.
847 This study investigated the long-term deformation and coseismic uplift on the Boso Peninsula
848 by using the observed geometry of PHS through seismic surveys. The long-term deformation
849 pattern correlates the residual resulting from asymmetry between co- and interseismic
850 deformations, namely the elevation distribution of Holocene marine terraces. The presence of a
851 subducted seamount beneath the southern part of the Boso Peninsula, as indicated by the seismic
852 survey conducted by Tsumura et al. (2009), was taken into account in the modeling. The
853 employment of subducted seamount geometry led an uplift concentration at the southernmost tip
854 of the Boso Peninsula. The simulated uplift rate was consistent with the estimated long-term uplift
855 rate derived from the height of the Holocene highest terrace in this region. Furthermore, by
856 incorporating coupling patches based on geodetic observations, the model also simulated a
857 concentration of coseismic uplift at the southernmost tip of the Boso Peninsula, which corresponds
858 to historical records.
859 The observation of the Numa terraces in the Boso Peninsula, with irregular formation intervals
860 despite comparable relative heights, highlights the complexity of the rupture history along the
861 Sagami Trough. It indicates that a more comprehensive rupture scenario is needed to explain the
862 geological and geodetic observations, including marine terrace distribution, displacements of
863 historical earthquakes, and present deformation observation from GNSS.
864 The verification of this study demonstrated significant differences in internal mechanical
865 consistency between MSPM and conventional models. However, when compared to surface
866 observations, the variations were negligible compared to the observational errors. Nevertheless,
867 compared to the traditional first-order approximation approach, which unconditionally assigns
868 uniform slip on the plate interface, the use of MSPM would reduce the potential for
869 misunderstandings in interpreting deformations and movements in subduction zones. Furthermore,
870 MSPM can reproduce more realistic behaviors in simulations of interseismic coupling and
871 coseismic ruptures (Herman and Govers, 2020; Lindsey et al., 2021), without increasing the
872 number of free parameters. Therefore, the utilization of the MSPM model would be recommended
873 for interpreting future short-term deformations in subduction zones.
874 The distinction between MSPM and the elastic/viscoelastic model lies in their treatment of
875 viscoelastic relaxation within the asthenosphere. MSPM assumes an elastic half-space and does
876 not explicitly simulate viscoelastic relaxation, whereas the elastic/viscoelastic model incorporates
877 viscoelastic behavior. While the elastic/viscoelastic model allows for a more realistic
878 representation of the asthenosphere's viscoelastic relaxation, it faces limitations inaccurately
879 simulating subduction with irregular plate interface geometries because it cannot directly calculate
880 the stress change on the slip surface. In contrast, MSPM has an ability to approximate complete
881 relaxation of stress in the asthenosphere over time by imposing a boundary condition that enforces
882 zero stress accumulation on LAB. This modeling approach, which accommodates complex
883 subduction geometries, offer as optimal combination of the models used in this study, unlike the
884 horizontal two-layered model.
885 Despite the long efforts to understand the earthquake recurrence history through the analysis
886 of vertical deformation recorded in coastal landforms, model explanations have faced challenges
887 in encompassing observations at various scales. Specifically, the relationship between Holocene
888 marine terraces and coseismic uplifts may have been overestimated due to their apparent
889 correlation. The findings of this study have shed light on the significant influence of subducted

seamounts on permanent deformation around subduction zones, prompting a reevaluation of the interpretation of marine terrace distributions. It has become evident that marine terraces are influenced not only by coseismic uplift but also by interseismic and long-term deformations, which necessitates a proper assessment of the subduction mechanism and plate interface geometry in order to infer the past rupture history accurately.

Acknowledgments

The authors would like to thank anonymous reviewers for thorough revies and insightful comments. The MCS reflection data shown in Figure 2b can be requested through JAMSTEC Seismic Survey Database (https://doi.org/10.17596/0002069). The topography data used in Figures 1 and 2a are the 30-arc sec General Bathymetric Chart of the Oceans (GEBCO) data (The GEBCO_2022 Grid). We used the DEM Viewer Blender application for the visualization of Figure 2a (https://doi.org/10.5281/zenodo.7091899) utilizing the coloring method by Chiba et al. (2008). This study was supported by the Ministry of Education, Culture, Sports, Science and Technology (MEXT) of Japan, under its Earthquake and Volcano Hazards Observation and Research Program.

References

Ando, R., Kaneko, Y. (2018). Dynamic Rupture Simulation Reproduces Spontaneous Multifault Rupture and Arrest During the 2016 Mw 7.9 Kaikoura Earthquake. Geophysical Research Letters, 45, 12875–12883. https://doi-org/10.1029/2018GL080550

Bessat, A., Duretz, T., Hetényi, G., Pilet, S., Schmalholz, S. M., (2020). Stress and deformation mechanisms at a subduction zone: insights from 2-D thermomechanical numerical modelling. Geophysical Journal International, 221, 1605–1625. https://doi.org/10.1093/gji/ggaa092

Briggs, R. W., Sieh, K., Meltzner, A. J., Natawidjaja, D., Geletzka, J., Suwargadi, B., et al. (2006). Deformation and Slip Along the Sunda Megathrust in the Great 2005 Nias-Simeulue Earthquake. Science, 311, 1897–1901, https://doi.org/10.1126/science.1122602

Briggs, R. W., Sieh, K., Amidon, W. H., Geletzka, J., Prayudi, D., Suprihanto, I.. et al. (2008). Persistent elastic behavior above a megathrust rupture patch: Nias island, West Sumatra. Journal of Geophysical Research, 113, B12406. https://doi.org/10.1029/2008JB005684

Chiba, T., Kaneta, S.-I., Suzuki, Y. (2008). Red relief image map: new visualization method for three dimensional data. The International Archives of the Photogrammetry, Remote Sensing and Spatial Information Sciences, 37, 1071-1076

Clark, K. J., Nissen, E. K., Howarth, J. D., Hamling I. J., Mountjoy J. J., Ries, W. F., et al., (2017). Highly variable coastal deformation in the 2016 MW7.8 Kaikōura earthquake reflects rupture complexity along a transpressional plate boundary. *Earth and Planetary Science Letters*, **474**, 334–344. https://doi.org/10.1016/j.epsl.2017.06.048

DeMets, C., Gordon, R.G., Argus, D.F., Stein, S. (1994). Effect of recent revisions to the geomagnetic reversal time scale on estimates of current plate motions, Geophysical Research Letters, 21, 2191–2194. https://doi.org/10.1029/94GL02118

Dominguez, S., Lallemand, S. E., Malavieille, J., von Huene, R., (1998). Upper plate deformation associated with seamount subduction, *Tectonophysics*, **293**, 207–224. https://doi.org/10.1016/S0040-1951(98)00086-9

Dominguez, S., Malavielle, J., Lallemand, S. E. (2000). Deformation of accretionary wedges in response to seamount subduction- Insights from sandbox experiments, *Tectonics*, **19**, 182–196. https://doi.org/10.1029/1999TC900055

Fukahata, Y., Matsu'ura, M. (2005). General expressions for internal deformation fields due to a dislocation source in a multilayered elastic half-space. *Geophysical Journal International*, **161**, 507-521. https://doi.org/10.1111/j.1365-246X.2005.02594.x

Fukahata, Y., Matsu'ura, M. (2006). Quasi-static internal deformation due to a dislocation source in a multilayered elastic/viscoelastic half-space and an equivalence theorem. *Geophysical Journal International*, **166**, 418–434. https://doi.org/10.1111/j.1365-246X.2006.02921.x

Fukahata, Y., Matsu'ura, M. (2016). Deformation of island-arc lithosphere due to steady plate subduction. *Geophysical Journal International*, **204**, 825–840. https://doi.org/10.1093/gji/ggv482

Gardner, T., Marshall, J., Merritts, D., Bee, B., Burgette, R., Burton, E., et al. (2001). Holocene forearc block rotation in response to seamount subduction, southeastern Península de Nicoya, Costa Rica, *Geology*, **29**, 151–154. https://doi.org/10.1130/0091-7613(2001)029<0151:HFBRIR>2.0.CO;2

Hashima, A., Takada, Y., Fukahata, Y., Matsu'ura, M. (2008). General expressions for internal deformation due to a moment tensor in an elastic/viscoelastic multilayered half-space, *Geophysical Journal International*, **175**, 992-1012. https://doi.org/10.1111/j.1365-246X.2008.03837.x

Hashima, A., Fukahata, Y., Hashimoto, C., Matsu'ura, M. (2014). Quasi-static strain and stress fields due to a moment tensor in elastic-viscoelastic layered half-space. Pure and Applied Geophysics, 171, 1669‑1693. https://doi.org/10.1007/s00024-013-0728-0

Hashimoto C., Fukui K., Matsu'ura M. (2004). 3-D modelling of plate interfaces and numerical simulation of long-term crustal deformation in and around Japan. *Pure and Applied Geophysics*, **161**, 2053–2068, https://doi.org/10.1007/s00024-004-2548-8

Hashimoto, C., Terakawa, T. (2018). Stress data inversion to estimate collision rate distribution and its application to the Izu Peninsula, Japan. *Tectonophysics*. **744**, 47–57. https://doi.org/10.1016/j.tecto.2018.06.001

Herman, M. W., Furlong, K. P., Govers, R. (2018). The accumulation of slip deficit in subduction zones in the absence of mechanical coupling: Implications for the behavior of megathrust earthquakes. *Journal of Geophysical Research: Solid Earth*, 123, 8260–8278. https://doi.org/10.1029/2018JB016336

Herman, M. W., Govers, R. (2020). Locating fully locked asperities along the South America subduction megathrust: A new physical interseismic inversion approach in a Bayesian framework. *Geochemistry, Geophysics, Geosystems*, **21**, e2020GC009063. https://doi.org/10.1029/2020GC009063

Hirose, F., Nakajima, J., Hasegawa, A. (2008) Three-dimensional velocity structure and configuration of the Philippine Sea slab beneath Kanto District, central Japan, estimated by

double-difference tomography: *Zisin*, **60**, p. 128–138, https://doi.org/10.4294/zisin.60.123 (in Japanese with English abstract).

Johnson, K. M., Segall, P. (2004). Viscoelastic earthquake cycle models with deep stress-driven creep along the San Andreas fault system. *Journal of Geophysical Research*, **109**, B10403, https://doi:10.1029/2004JB003096

Johnson, K. M., Fukuda, J. (2010), New methods for estimating the spatial distribution of locked asperities and stress-driven interseismic creep on faults with application to the San Francisco Bay Area, California, *Journal of Geophysical Research*, **115**, B12408, https://doi.org/10.1029/2010JB007703.

Kanda, R. V. S., Simons, M. (2010). An elastic plate model for interseismic deformation in subduction zones, *Journal of Geophysical Research*, **115**, B03405, https://doi.org/10.1029/2009JB006611

Kanda, R. V. S., Simons, M. (2012). Practical implications of the geometrical sensitivity of elastic dislocation models for field geologic surveys, *Tectonophysics*, **560–561**, 94–104. https://doi.org/10.1016/j.tecto.2012.06.040

Kawakami, S., Shishikura, M. (2006). Geological Map 1:50,000. Tateyama, Geological Survey of Japan, (in Japanese with English abstract).

Kimura H., Kasahara, K., Takeda, T. (2009). Subduction process of the Philippine Sea Plate off the Kanto district, central Japan, as revealed by plate structure and repeating earthquakes. Tectonophysics, 472, 18–27. http://dx.doi.org/10.1016/j.tecto.2008.05.012

Kodaira, S., Takahashi, N., Nakanishi, A., Miura, S., Kaneda, Y. (2000). Subducted Seamount Imaged in the Rupture Zone of the 1946 Nankaido Earthquake, Science, 289, 104–106. https://doi.org/10.1126/science.289.5476.104

Komatsubara, T. (2017). Some facts on activity of southern part of the Kamogawa Lowland fault zone, Boso peninsula, central Japan, Active Fault Research, 46, 17‑25. (in Japanese with English abstract). https://doi.org/10.11462/afr.2017.46_17

Komori, J., Ando, R., Shishikura, M. (2020). Cluster analysis of marine terraces and quantitative seismotectonic interpretation of the Boso Peninsula, central Japan. *Journal of Geophysical Research: Solid Earth*, **125**, e2019JB019211. https://doi.org/10.1029/2019JB019211

Komori, J., Shishikura, M., Ando, R., Yokoyama, Y., Miyairi, Y. (2021). The history of the great Kanto earthquakes, central Japan: A Bayesian approach to age estimation of marine terraces. *Quaternary Science Reviews*, **272**, 107217, https://doi.org/10.1016/j.quascirev.2021.107217

Lindsey, E.O., Mallick, R., Hubbard, J.A., Hubbard, J. A., Bradley, K. E., Almedia, R. V., Moore, J. D. P., et al. (2021). Slip rate deficit and earthquake potential on shallow megathrusts. *Nature Geoscience*. **14**, 321–326. https://doi.org/10.1038/s41561-021-00736-x

Litchfield, N. J., Clark, K. J., Cochran, U. A., Palmer, A. S., Mountjoy, J., Mueller, C., et al., (2020). Marine terraces reveal complex near-shore upper-plate faulting in the northern Hikurangi margin, New Zealand. *Bulletin of the Seismological Society of America*, **110**, 825–849, https://doi.org/10.1785/0120190208

Matsuda, T., Ota, Y., Ando, M., Yonekura, N. (1978). Fault mechanism and recurrence time of major earthquakes in southern Kanto district, Japan, as deduced from coastal terrace data.

Geological Society of America Bulletin, **89**, 1610-1618. https://doi.org/10.1130/0016-7606(1978)89%3C1610:FMARTO%3E2.0.CO;2

Matsu'ura, M, Sato, T. (1989). A dislocation model for the earthquake cycle at convergent plate boundaries. Geophysical Journal International, **96**, 23–32, https://doi.org/10.1111/j.1365-246X.1989.tb05247.x

Miura, S., Yamashita, M., Takahashi, N., No, T., Kodaira, S., Nozaki, K., Kobayashi, R. (2009). Multichannel seismic profiles crossing source regions of megathrust earthquakes and slow slip events off-Boso, central Japan, American Geophysical Union 2009 Fall Meeting, NH31A-1093

Miyakawa, A., Noda, A., Koge, H. (2022). Evolution of the geological structure and mechanical properties due to the collision of multiple basement topographic highs in a forearc accretionary wedge: insights from numerical simulations. Progress in Earth and Planetary Science, 9, 1. https://doi.org/10.1186/s40645-021-00461-4

Nakajima, T., Makimoto, H., Hirayama, J., Tokuhashi, S. (1981). Geology of the Kamogawa district. Quadrangle Series, scale 1:50,000, Geological Survey of Japan, 107p. (in Japanese with English Abstract)

Nakata, T., Koba, M., Imaizumi, T., Jo, W., Matsumoto, H. Suganuma, T. (1980). Holocene marine terraces and seismic crustal movements in the southern part of Boso Peninsula, Kanto, Japan. *Geographical Review of Japan, Series A*, **53**, 29-44, (in Japanese with English abstract and figure captions). https://doi.org/10.4157/grj.53.29

Nikkhoo, M. and Walter, T. R. (2015). Triangular dislocation: an analytical, artefact-free solution. *Geophysical Journal International*, **201**, 1119–1141. https://doi.org/10.1093/gji/ggv035

Ninis, D., Howell, A., Little, T., Litchfield, N. (2023). Causes of permanent vertical deformation at subduction margins: Evidence from late Pleistocene marine terraces of the southern Hikurangi margin, Aotearoa New Zealand. Frontiers in Earth Science. 11:1028445. https://doi.org/10.3389/feart.2023.1028445

Noda, A., Hashimoto, C., Fukahata, Y., Matsu'ura, M. (2013). Interseismic GPS strain data inversion to estimate slip-deficit rates at plate interfaces: application to the Kanto region, central Japan. *Geophysical Journal International*, **193**, 61–77, https://doi.org/10.1093/gji/ggs129

Noda, A., Miyauchi, T., Sato, T., Matsu'ura, M. (2018). Modelling and simulation of Holocene marine terrace development in Boso Peninsula, central Japan. *Tectonophysics*, **731**, 139–154. https://doi.org/10.1016/j.tecto.2018.03.008

Nyst, M., Nishimura, T., Pollitz, F. F., Thatcher, W. (2006), The 1923 Kanto earthquake reevaluated using a newly augmented geodetic data set, Journal of. Geophysical Research, 111, B11306, doi:10.1029/2005JB003628.

Plafker, G. (1969). Tectonics of the March 27, 1964 Alaska earthquake: U.S. Geological Survey Professional Paper 543–I, 74 p., 2 sheets, scales 1:2,000,000 and 1:500,000. https://pubs.usgs.gov/pp/0543i/

Pollitz, F. F., Pichon, X. Le, Lallemant, S. J. (1996). Shear partitioning near the central Japan triple junction: The 1923 Great Kanto earthquake revisited: II, *Geophysical Journal International*, **126**, 882–892. https://doi.org/10.1111/j.1365-246X.1996.tb04710.x

Ramos N. T., Tsutsumi, H. (2010). Evidence of large prehistoric offshore earthquakes deduced from uplifted Holocene marine terraces in Pangasinan Province, Luzon Island, Philippines. *Tectonophysics*, **495**, 145–158. https://doi.org/10.1016/j.tecto.2010.08.007

Romanet, P., Sato, D. S. K., Ando, R. (2020). Curvature, a mechanical link between the geometrical complexities of a fault: application to bends, kinks and rough faults. *Geophysical Journal International*, **223**, 211–232. https://doi: 10.1093/gji/ggaa308

Sagiya, T. (2004). Interplate coupling in the Kanto District, central Japan, and the Boso Silent earthquake in May 1996, *Pure and Applied Geophysics*, **161**, 11-12, 2601-2616. https://doi.org/10.1007/s00024-004-2566-6

Sato, H., Hirata, N., Koketsu, K., Okaya, D., Abe, S., Kobayashi, R., et al. (2005). Earthquake source fault beneath Tokyo. *Science*, **309**, 462–464. DOI: 10.1126/science.1110489

Sato, T., Matsu'ura, M. (1988) A kinematic model for deformation of the lithosphere at subduction zones, *Journal of Geophysical Research*, **93**, 6410–6418. https://doi.org/10.1029/JB093iB06p06410

Sato, T., Higuchi, H., Miyauchi, T., Endo, K., Tsumura, N., Ito, T., et al. (2016). The source model and recurrence interval of Genroku-type Kanto earthquakes estimated from paleo-shoreline data. *Earth, Planets and Space*, **68**, 1–17. https://doi.org/10.1186/s40623-016-0395-3

Savage, J. C. (1983). A dislocation model of strain accumulation and release at a subduction zone. *Journal of Geophysical Research*, **88**, 4984–4996. https://doi.org/10.1029/JB088iB06p04984

Seno, T., Stein, S., Gripp, A. E. (1993). A model for the motion of the Philippine Sea Plate consistent with NUVEL-1 and geological data. *Journal of Geophysical Research: Solid Earth*, **98**, 17941‑17948. https://doi.org/10.1029/93JB00782

Shimazaki, K., Nakata, T. (1980). Time-predictable recurrence model for large earthquakes. *Geophysical Research Letters*, **7**, 279–282. https://doi.org/10.1029/GL007i004p00279

Shishikura, M. (2014). History of the paleo-earthquakes along the Sagami Trough, central Japan: Review of coastal paleo-seismological studies in the Kanto region. *Episodes*, **37**, 246–257. https://doi.org/10.18814/epiiugs/2014/v37i4/004

Sun, T., Saffer, D., Ellis, S. (2020). Mechanical and hydrological effects of seamount subduction on megathrust stress and slip. Nature Geoscience, 13, 249–255. https://doi.org/10.1038/s41561-020-0542-0

Thompson, B., Vasyura-Bathke, H., Howell, A., Meade, B. (2023). Python CPU and GPU accelerated TDEs, over 100 million TDEs per second! tbenthompson/cutde: v23.6.25 (v23.6.25). Zenodo. https://doi.org/10.5281/zenodo.8080078

Tsumura, N., Komada, N., Sano, J., Kikuchi, S., Yamamoto, S., Ito, T., et al. (2009). A bump on the upper surface of the Philippine Sea plate beneath the Boso Peninsula, Japan inferred from seismic reflection surveys: A possible asperity of the 1703 Genroku earthquake. *Tectonophysics*, **472**, 39–50. https://doi.org/10.1016/j.tecto.2008.05.009

Usami, T., Ishi, H., Imamura, T., Takemura, M., Matsuura, R. (2013). Materials for comprehensive list of destructive earthquakes in Japan. Univ. Tokyo Press (in Japanese).

van Rijsingen, E., Lallemand, S., Peyret, M., Arcay, D., Heuret, A., Funiciello, F., Corbi, F., (2018). How subduction interface roughness influences the occurrence of large interplate earthquakes. Geochemistry Geophysics Geosystems, 19 (8), 2342–2370. http://dx.doi.org/10.1029/2018GC007618

Wang K, Bilek L. (2011). Do subducting seamounts generate or stop large earthquakes? *Geology*, **39**, 819–822. https://doi.org/10.1130/G31856.1

Wang, Y., Shyu, J.B.H., Sieh, K., Chiang, H.-W., Wang, C.-C., Aung, T., et al. (2013). Permanent upper plate deformation in western Myanmar during the great 1762 earthquake: Implications for neotectonic behavior of the northern Sunda megathrust. *Journal of Geophysical Research: Solid Earth*, **118**, 1277-1303. 10.1002/jgrb.50121

Watanabe, A. (1929). Preliminary Note on the Coastal Terraces of the Southern Parts of Bôsô Peninsula, *Geographical review of Japan*, **5**, 119–126. https://doi.org/10.4157/grj.5.119

Wessel, P., Sandwell, D. T., Kim, S.-S. (2010). The Global Seamount Census. *Oceanography*, **23**, 24–33. https://doi.org/10.5670/oceanog.2010.60

Wesson, R., Melnick, D., Cisternas, M., Moreno, M., Ely, L., L. (2015). Vertical deformation through a complete seismic cycle at Isla Santa María, Chile. Nature Geoscience, 8, 547–551. https://doi.org/10.1038/ngeo2468

Figure 1. Survey region of this study and geological observations. (a) Tectonic setting of the Sagami Trough. The red meshed area indicates the estimated source region of the historical Kanto earthquakes (Sato et al., 2005; Sato et al., 2016). (b) Distribution of the Numa terraces after Komori et al. (2020). Right panels show the elevation distribution of the Numa terraces at each reference point, indicated by triangles in the left map.

Figure 2. (a) Bathymetry map around the survey region and the profile lines of the previous reflection surveys (Sato et al., 2005; Kimura et al., 2009; Miura et al., 2009; Tsumura et al., 2009). The blue contour lines indicate the estimated depth of upper PHS by Tsumura et al. (2009), where the dark-blue straight lines are the survey profiles. The red lines indicate the inland active faults, where KTFZ stands for Kamogawa-teichi fault zone. (b) Post stack time migrated reflection image of the BOS-1C profile (Miura et al., 2009). Solid black line is our interpretation of the plate interface. Triangles indicate the positions of intersection with the survey lines of Tsumura et al. (2009).

Figure 3. Schematic illustration of subduction models. (a) General geometrical setting of plate subduction. (b) Schematic representation of the imposed steady state assessed from the back-slip model, following the interpretation by Kanda and Simons (2010). (c) Slip configuration for the steady state of ESPM (Kanda and Simons, 2010). Uniform slip is imposed on the entire plate interfaces (double arrows). (d) Schematic structure illustration of the elastic/viscoelastic model. Uniform slip is imposed on the plate interface above the LAB. (e) Boundary conditions of MSPM. Black solid arrows and white arrows indicate the interfaces where uniform slip is imposed (Γ_D: area of displacement boundary condition) and no shear stress change occurs (Γ_S:area of stress boundary condition), respectively.

Figure 4. Geometry setting of the simple plate subduction model. (a) Plan view of the upper plate interface. The black lines indicate depth contours at 2 km interval. A conical-shaped bump

with a height of 8 km is positioned at a depth of 10 km. The red rectangle indicates the rupture area and coupling patch in the earthquake sequence examination (Figure 8) (b) Cross-sectional view of the model geometry. The lower plate interface is set with a thickness H for ESPM and MSPM. (c) Schematic illustration of the superposition calculation used in the elastic/viscoelastic model. Refer to the main text for an explanation of this assumption. (d) Division of plate interfaces and boundary conditions in the earthquake sequence model using MSPM. The red and black broken lines correspond to the coupling patch and transition zone, respectively, applied during the interseismic period. The stress boundary condition is applied to the entire Γ_S during steady-state and coseismic events. The displacement boundary condition is applied to Γ_D during steady-state and the interseismic period.

Figure 5. Geometry setting of the model simulation for the Sagami Trough subduction zone. The contour is the depth distribution of the upper plate interface of PHS, referring to Hashimoto et al. (2004), Hirose et al. (2008), and Tsumura et al. (2009). The black rectangle indicates the area of stress boundary condition, including a coupling patch for the earthquake sequence model, denoted by the red rectangle. Outside of the AOS is steady slip area, where uniform slip is imposed in the direction indicated by the arrow.

Figure 6. Simulation results of the subduction models with the simple plate geometry. (a and b) Results of ESPM. (c and d) Results of the elastic/viscoelastic model. (e and f) Results of MSPM. (a, c, and e) Displacements (arrows) and stress change distribution (color map) showing the overall cross-sectional view. Black color represents greater than 4.5 MPa/m, namely singular value. The white solid lines and dashed lines depict the plate interfaces and the depth of LAB, respectively. The arrows outside the slab (bluish colored) are exaggerated by ten times than those inside the slab. (b, d, and f) Close-up view around the bump geometry. The extension is shown by the rectangle in the overall view. (g) Slip rate distribution on the plate interface using MSPM, relative to unit slip rate V. Contour lines indicate the depth of the plate interface by 2 km interval, same as Figure 4a.

Figure 7. (a and b) Vertical and horizontal displacement distribution in each model. These results correspond to the arrows on the surface depicted in Figures 6 a, c, and e. Positive value indicates movements towards the subduction direction in (b). (c) Vertical displacement distributions with different bump geometries. The line colours correspond to the geometries of subducted seamounts. MSPM model was used for these simulations.

Figure 8. Transition of vertical displacements resulting from the earthquake sequence models. The red portion of the plate interface geometry indicates range pf the rupture area (ESPM and Elastic/viscoelastic model) and coupling patch (MSPM), as shown in Figure 4. Red lines present the coseismic vertical deformation at $t = 0$ and transits into the terminal deformation pattern at $t = t_o$ depicted by the green lines. Yellow lines represent the snapshots of this transition at every 1/5 t_o. The differences between red and green lines are interseismic total deformation, which is depicted by the blue lines. The shaded portions of the green lines indicate the residual uplift, where uplifts are observed both in coseismic and terminal deformation patterns.

Figure 9. Simulated deformation distributions using MSPM with the model geometry of the Sagami Trough subduction zone. (a) Vertical displacement rate distribution with the steady-state assumption. (b) Coseismic vertical deformation distribution with the coupling patch representing

the 1703 event, depicted by the red rectangle. (c) Comparison between the observed elevation distribution of the highest Holocene paleo-shoreline (Shishikura, 2014) and simulated vertical displacement rate. Observation points are displayed in (a). The amplitude of vertical displacement is calibrated assuming that the convergence rate and the age of the highest Holocene sea level are 35 mm/year and 7,000 BP. The vertical displacement is shifted by 5 meters reflecting the Holocene highstand.

Figures.

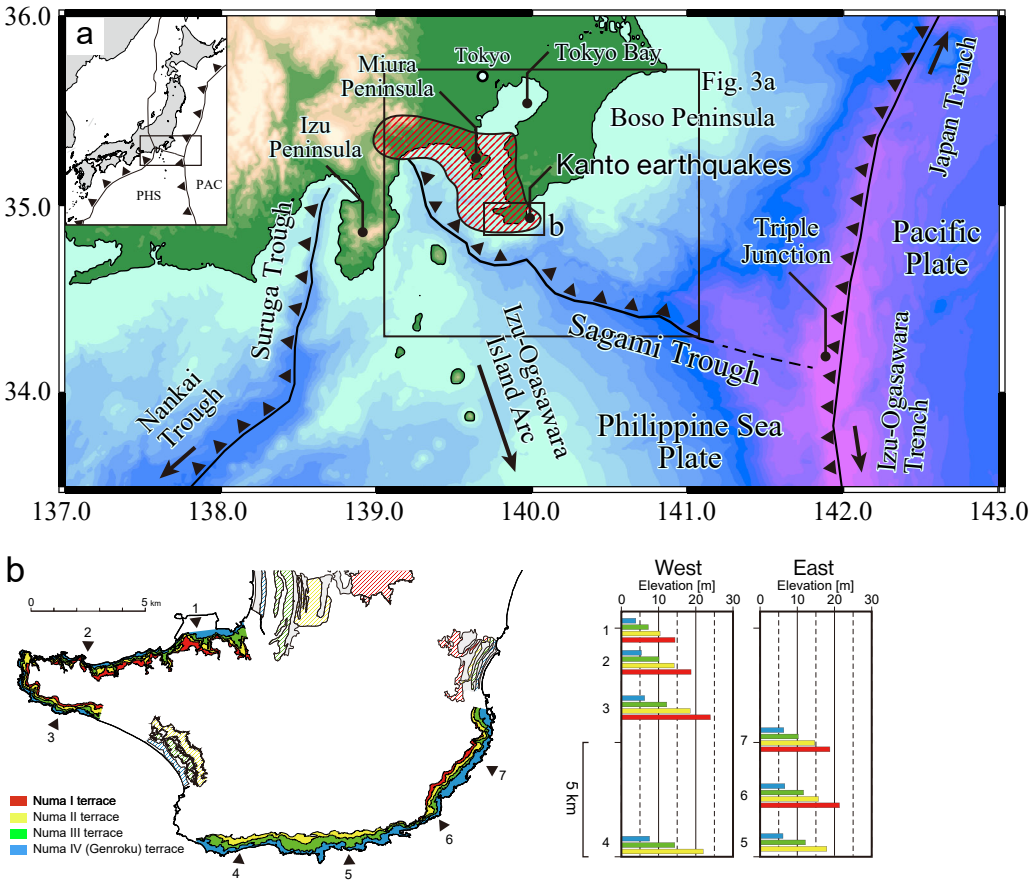

Figure 1. Survey region of this study and geological observations. (a) Tectonic setting of the Sagami Trough. The red meshed area indicates the estimated source region of the historical Kanto earthquakes (Sato et al., 2005; Sato et al., 2016). (b) Distribution of the Numa terraces after Komori et al. (2020). Right panels show the elevation distribution of the Numa terraces at each reference point, indicated by triangles in the left map.

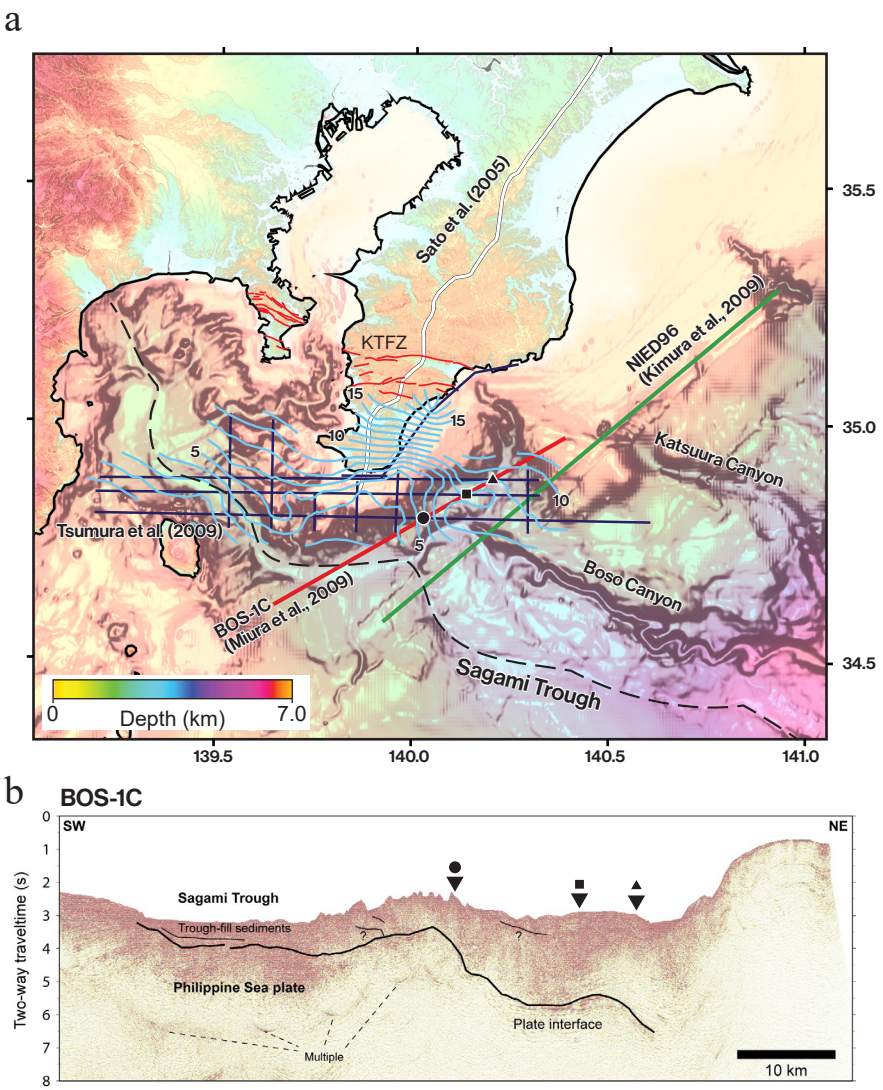

Figure 2. (a) Bathymetry map around the survey region and the profile lines of the previous reflection surveys (Sato et al., 2005; Kimura et al., 2009; Miura et al., 2009; Tsumura et al., 2009). The blue contour lines indicate the estimated depth of upper PHS by Tsumura et al. (2009), where the dark-blue straight lines are the survey profiles. The red lines indicate the inland active faults, where KTFZ stands for Kamogawa-teichi fault zone. (b) Post stack time migrated reflection image of the BOS-1C profile (Miura et al., 2009). Solid black line is our interpretation of the plate interface. Triangles indicate the positions of intersection with the survey lines of Tsumura et al. (2009).

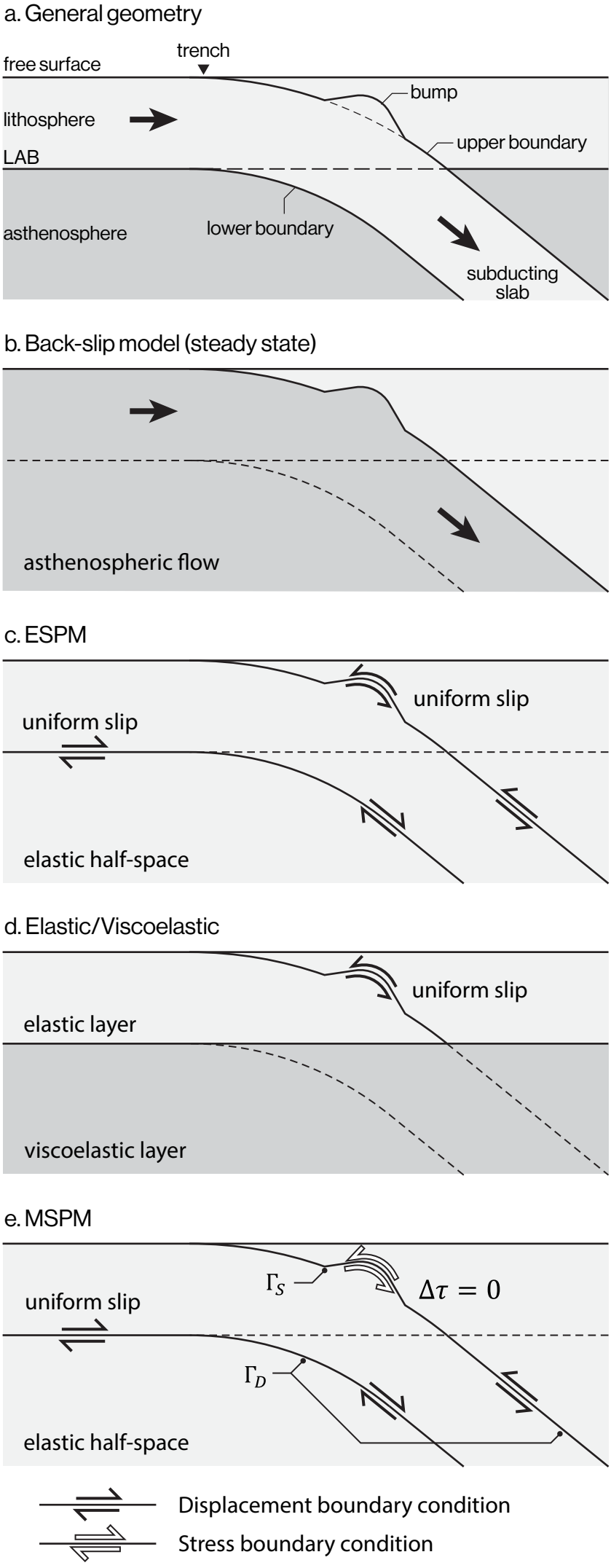

Figure 3. Schematic illustration of subduction models. (a) General geometrical setting of plate subduction. (b) Schematic representation of the imposed steady state assessed from the back-slip model, following the interpretation by Kanda and Simons (2010). (c) Slip configuration for the steady state of ESPM (Kanda and Simons, 2010). Uniform slip is imposed on the entire plate interfaces (double arrows). (d) Schematic structure illustration of the elastic/viscoelastic model. Uniform slip is imposed on the plate interface above the LAB. (e) Boundary conditions of MSPM. Black solid arrows and white arrows indicate the interfaces where uniform slip is imposed (Γ_D: area of displacement boundary condition) and no shear stress change occurs (Γ_S:area of stress boundary condition), respectively.

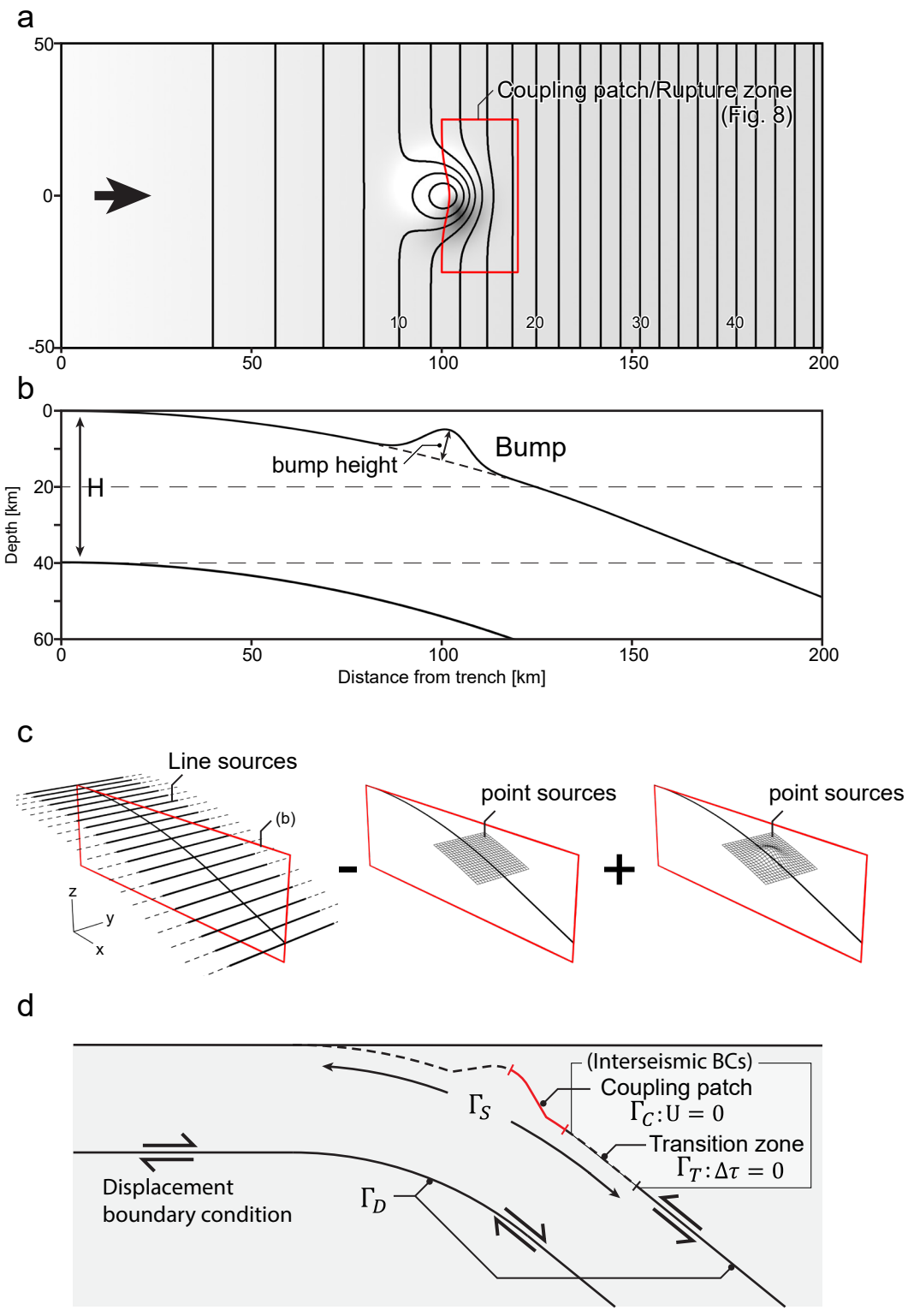

Figure 4. Geometry setting of the simple plate subduction model. (a) Plan view of the upper plate interface. The black lines indicate depth contours at 2 km interval. A conical-shaped bump with a height of 8 km is positioned at a depth of 10 km. The red rectangle indicates the rupture area and coupling patch in the earthquake sequence examination (Figure 8) (b) Cross-sectional view of the model geometry. The lower plate interface is set with a thickness H for ESPM and MSPM. (c) Schematic illustration of the superposition calculation used in the elastic/viscoelastic model. Refer to the main text for an explanation of this assumption. (d) Division of plate interfaces and boundary conditions in the earthquake sequence model using MSPM. The red and black broken lines correspond to the coupling patch and transition zone, respectively, applied during the interseismic period. The stress boundary condition is applied to the entire Γ_S during steady-state and coseismic events. The displacement boundary condition is applied to Γ_D during steady-state and the interseismic period.

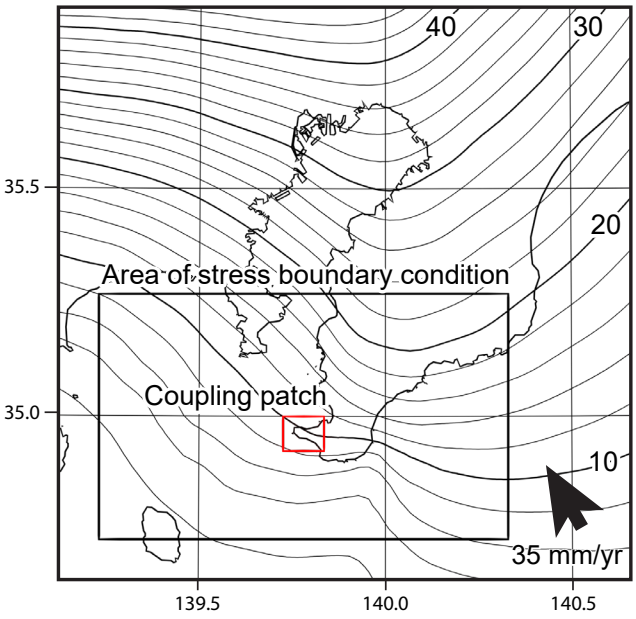

Figure 5. Geometry setting of the model simulation for the Sagami Trough subduction zone. The contour is the depth distribution of the upper plate interface of PHS, referring to Hashimoto et al. (2004), Hirose et al. (2008), and Tsumura et al. (2009). The black rectangle indicates the AOS, including a coupling patch for the earthquake sequence model, denoted by the red rectangle. Outside of the AOS is steady slip area, where uniform slip is imposed in the direction indicated by the arrow.

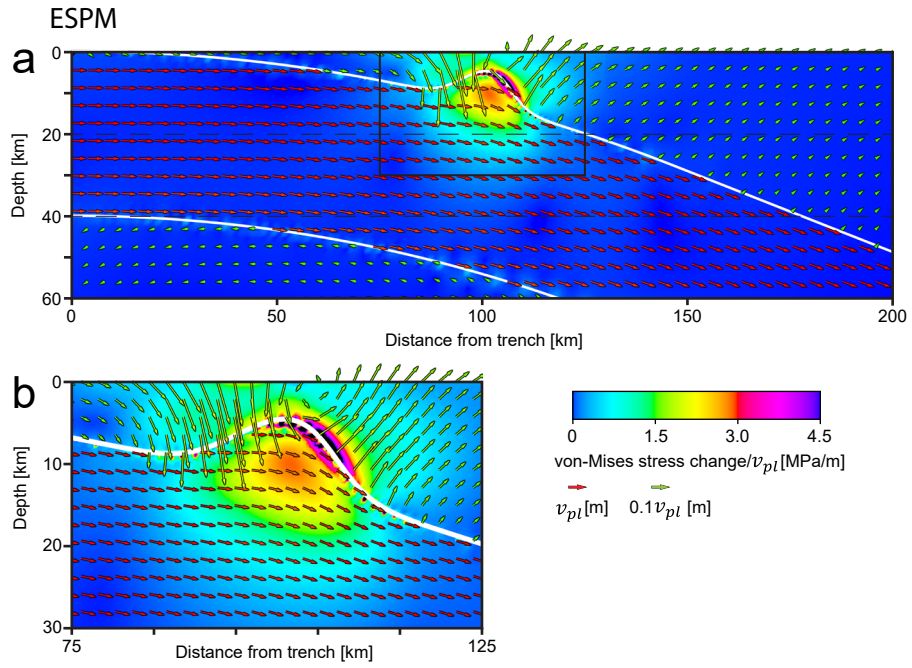

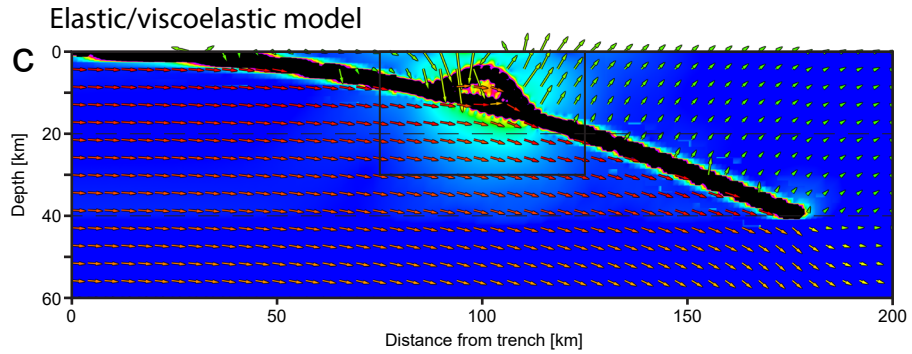

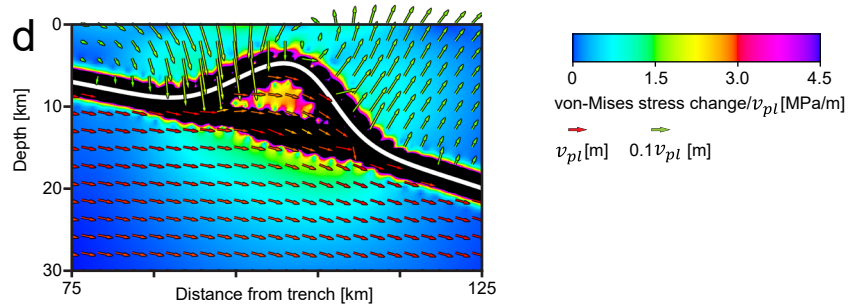

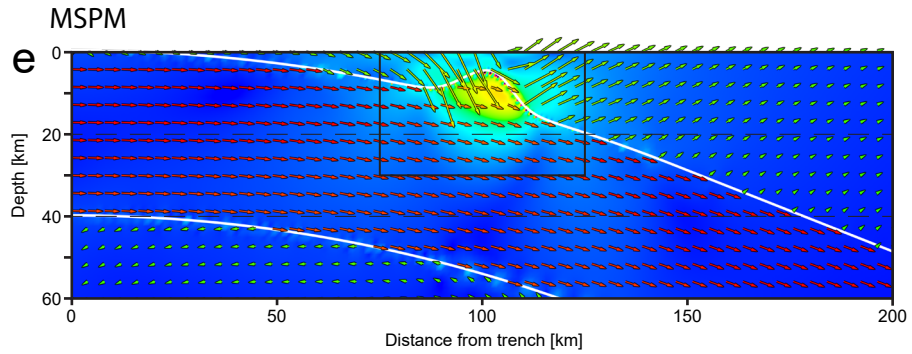

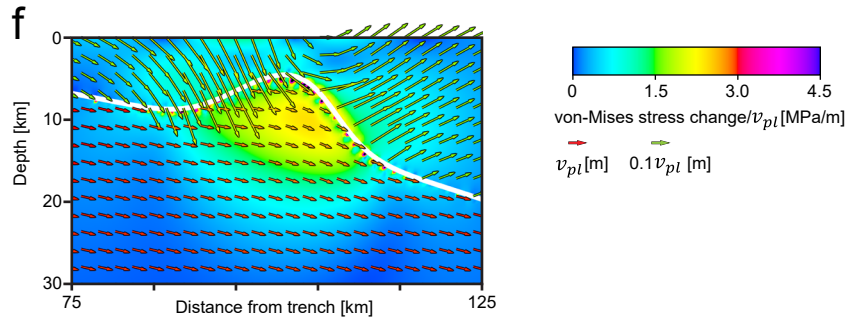

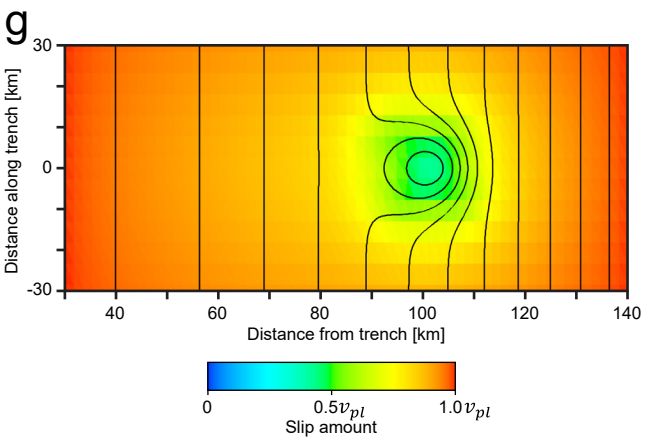

Figure 6. Simulation results of the subduction models with the simple plate geometry. (a and b) Results of ESPM. (c and d) Results of the elastic/viscoelastic model. (e and f) Results of MSPM. (a, c, and e) Displacements (arrows) and stress change distribution (color map) showing the overall cross-sectional view. Black color represents greater than 4.5 MPa/m, namely singular value. The white solid lines and dashed lines depict the plate interfaces and the depth of LAB, respectively. The arrows outside the slab (bluish colored) are exaggerated by ten times than those inside the slab. (b, d, and f) Close-up view around the bump geometry. The extension is shown by the rectangle in the overall view. (g) Slip rate distribution on the plate interface using MSPM, relative to unit slip rate V. Contour lines indicate the depth of the plate interface by 2 km interval, same as Figure 4a.

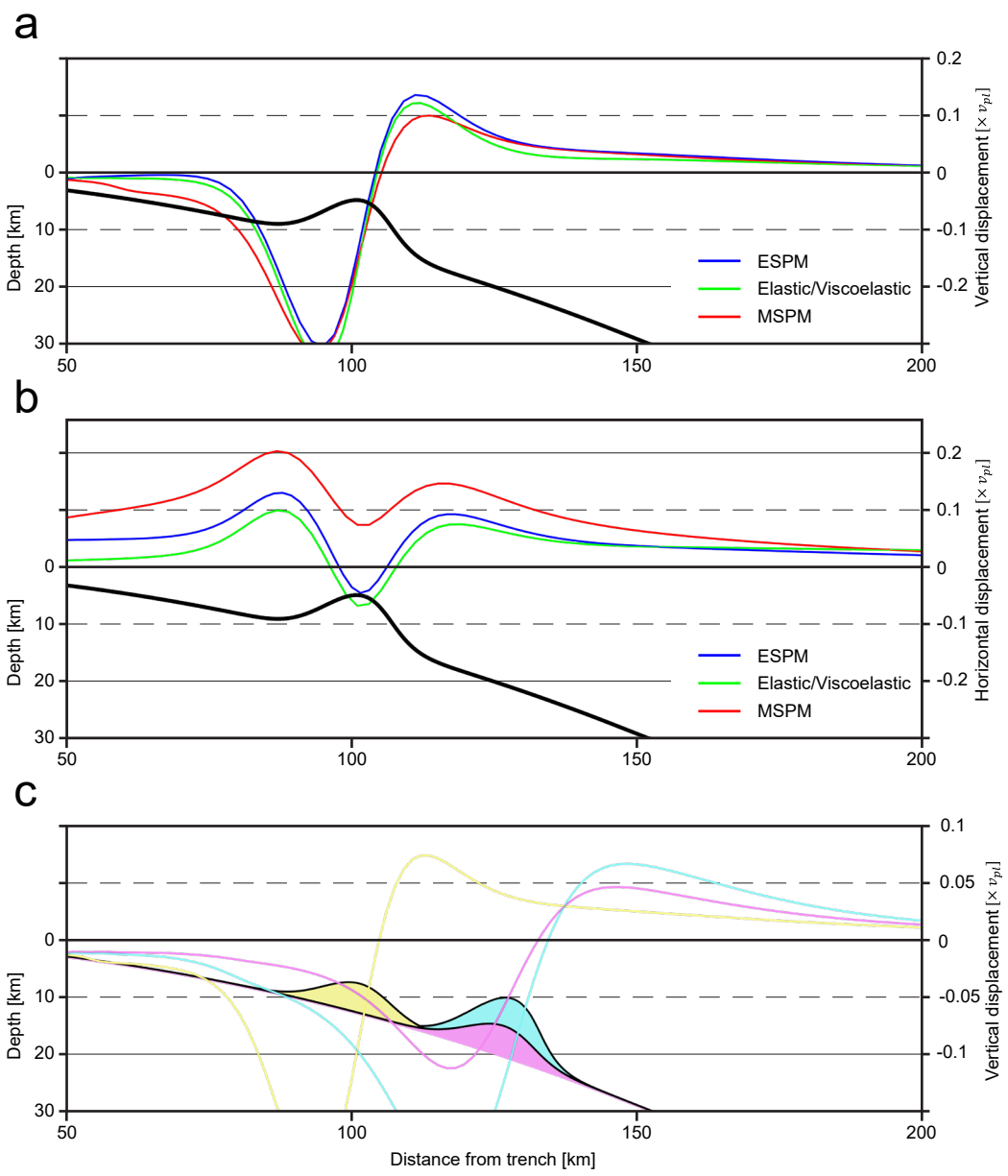

Figure 7. (a and b) Vertical and horizontal displacement distribution in each model. These results correspond to the arrows on the surface depicted in Figures 6 a, c, and e. Positive value indicates movements towards the subduction direction in (b). (c) Vertical displacement distributions with different bump geometries. The line colours correspond to the geometries of subducted seamounts. MSPM model was used for these simulations.

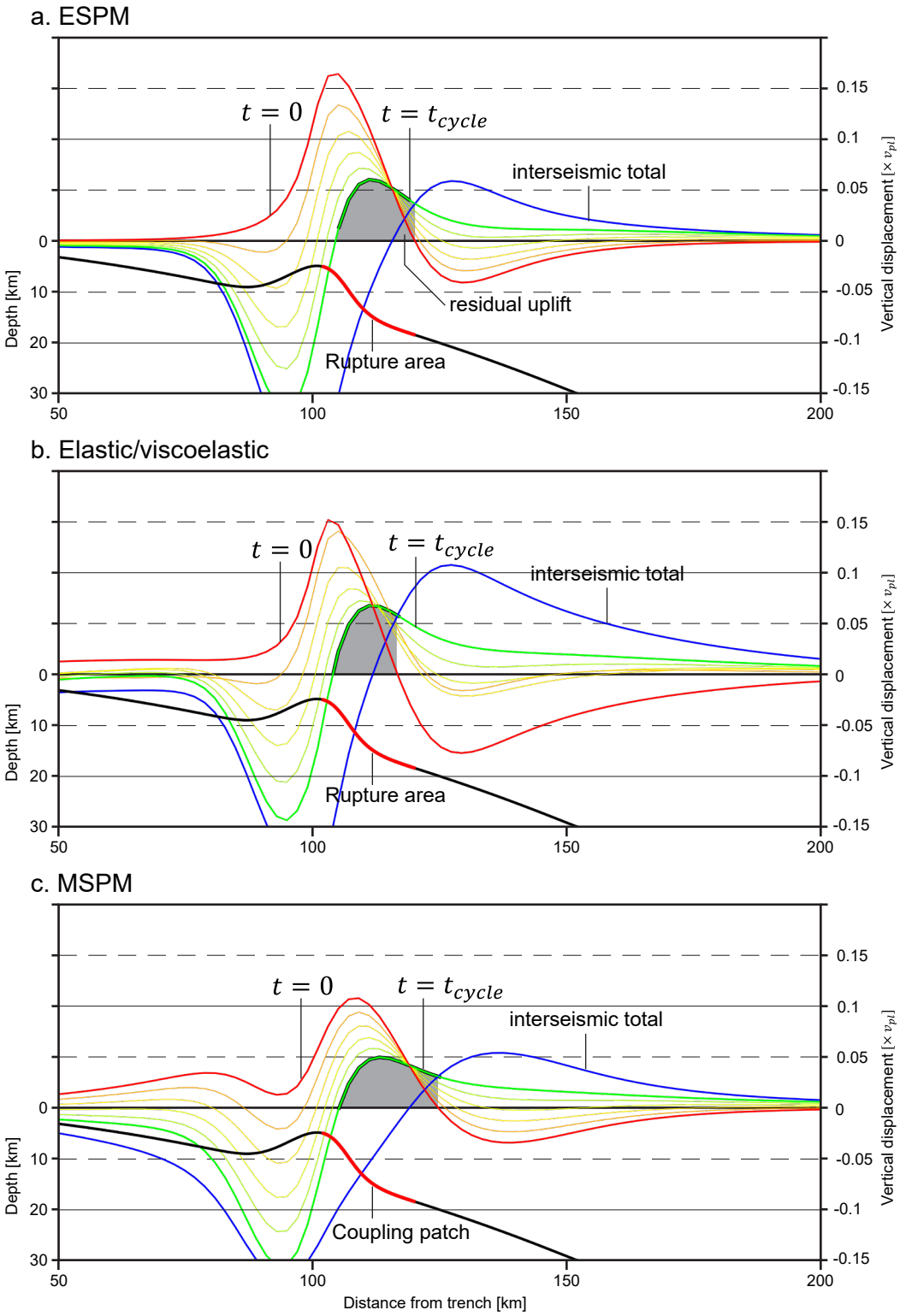

Figure 8. Transition of vertical displacements resulting from the earthquake sequence models. The red portion of the plate interface geometry indicates range pf the rupture area (ESPM and Elastic/viscoelastic model) and coupling patch (MSPM), as shown in Figure 4. Red lines present the coseismic vertical deformation at t=0 and transits into the terminal deformation pattern at t=t_cycle depicted by the green lines. Yellow lines represent the snapshots of this transition at every 1/5 t_cycle. The differences between red and green lines are interseismic total deformation, which is depicted by the blue lines. The shaded portions of the green lines indicate the residual uplift, where uplifts are observed both in coseismic and terminal deformation patterns.

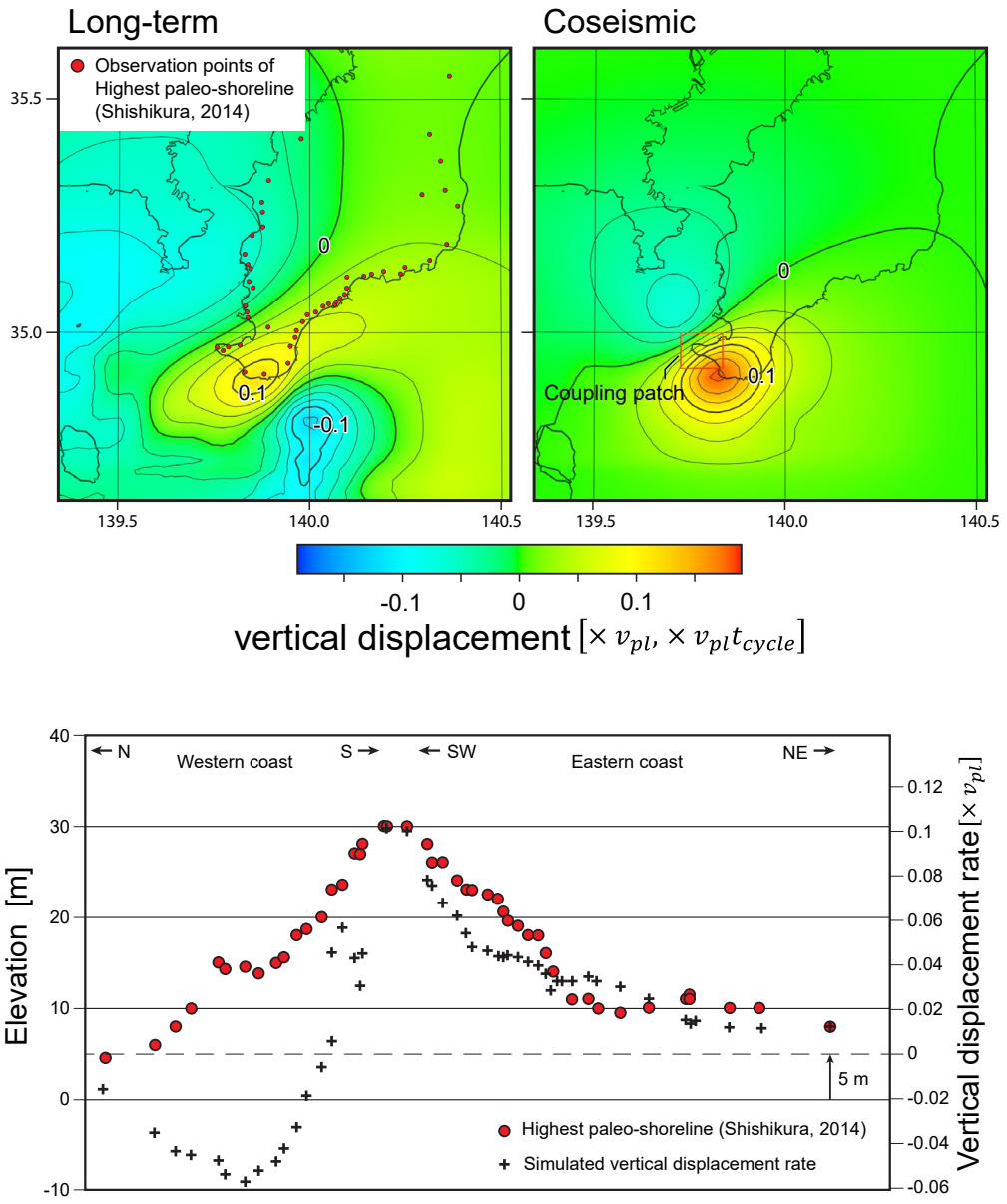

Figure 9. Simulated deformation distributions using MSPM with the model geometry of the Sagami Trough subduction zone. (a) Vertical displacement rate distribution with the steady-state assumption. (b) Coseismic vertical deformation distribution with the coupling patch representing the 1703 event, depicted by the red rectangle. (c) Comparison between the observed elevation distribution of the highest Holocene paleo-shoreline (Shishikura, 2014) and simulated vertical displacement rate. Observation points are displayed in (a). The amplitude of vertical displacement is calibrated assuming that the convergence rate and the age of the highest Holocene sea level are 35 mm/year and 7,000 BP. The vertical displacement is shifted by 5 meters reflecting the Holocene highstand.